



z -Transform Methods for the Optimal Design of One-Dimensional Layered Elastic Media

by Ani P. Velo, George A. Gazonas, and Takanobu Ameya

ARL-RP-287

January 2010

A reprint from the *SIAM Journal of Applied Mathematics*,
Vol. 70, No. 3, pp. 762–788, 2009.

NOTICES

Disclaimers

The findings in this report are not to be construed as an official Department of the Army position unless so designated by other authorized documents.

Citation of manufacturer's or trade names does not constitute an official endorsement or approval of the use thereof.

Destroy this report when it is no longer needed. Do not return it to the originator.

Army Research Laboratory

Aberdeen Proving Ground, MD 21005-5069

ARL-RP-287

January 2010

z -Transform Methods for the Optimal Design of One-Dimensional Layered Elastic Media

Ani P. Velo and Takanobu Ameya
University of San Diego

George A. Gazonas
Weapons and Materials Research Directorate, ARL

A reprint from the *SIAM Journal of Applied Mathematics*,
Vol. 70, No. 3, pp. 762–788, 2009.

REPORT DOCUMENTATION PAGE			<i>Form Approved</i> OMB No. 0704-0188		
Public reporting burden for this collection of information is estimated to average 1 hour per response, including the time for reviewing instructions, searching existing data sources, gathering and maintaining the data needed, and completing and reviewing the collection information. Send comments regarding this burden estimate or any other aspect of this collection of information, including suggestions for reducing the burden, to Department of Defense, Washington Headquarters Services, Directorate for Information Operations and Reports (0704-0188), 1215 Jefferson Davis Highway, Suite 1204, Arlington, VA 22202-4302. Respondents should be aware that notwithstanding any other provision of law, no person shall be subject to any penalty for failing to comply with a collection of information if it does not display a currently valid OMB control number. PLEASE DO NOT RETURN YOUR FORM TO THE ABOVE ADDRESS.					
1. REPORT DATE (DD-MM-YYYY) January 2010		2. REPORT TYPE Reprint		3. DATES COVERED (From - To) June 2008–July 2009	
4. TITLE AND SUBTITLE z-Transform Methods for the Optimal Design of One-Dimensional Layered Elastic Media			5a. CONTRACT NUMBER W911NF-07-D-0001		
			5b. GRANT NUMBER		
			5c. PROGRAM ELEMENT NUMBER		
6. AUTHOR(S) Ani P. Velo*, George A. Gazonas, and Takanobu Ameya*			5d. PROJECT NUMBER		
			5e. TASK NUMBER		
			5f. WORK UNIT NUMBER		
7. PERFORMING ORGANIZATION NAME(S) AND ADDRESS(ES) U.S. Army Research Laboratory ATTN: RDRL-WMM-D Aberdeen Proving Ground, MD 21005-5069			8. PERFORMING ORGANIZATION REPORT NUMBER ARL-RP-287		
9. SPONSORING/MONITORING AGENCY NAME(S) AND ADDRESS(ES)			10. SPONSOR/MONITOR'S ACRONYM(S)		
			11. SPONSOR/MONITOR'S REPORT NUMBER(S)		
12. DISTRIBUTION/AVAILABILITY STATEMENT Approved for public release; distribution is unlimited.					
13. SUPPLEMENTARY NOTES A reprint from the <i>SIAM Journal of Applied Mathematics</i> , Vol. 70, No. 3, pp. 762–788, 2009. Department of Mathematics and Computer Science, University of San Diego, 5998 Alcalá Park, San Diego, CA 92110					
14. ABSTRACT In this work, we develop a finite trigonometric series representation for the stress in amultilayered Goupillaud-type elastic strip subjected to transient Heaviside loading on one end while the other end is held fixed. This representation is achieved by means of the z-transform method and involves the so-called base angles. Generally, different layered designs could share the same set of base angles, and the more layers the design has, the more base angles are expected. Necessary conditions for the base angles and design parameters for any given design are described. As a result of the stress representation, we are able to identify optimal layered designs which provide the smallest stress amplitude. For two- and three-layered designs, for which the coefficients of the stress representation are easy to find, the optimization results are achieved using a custom-made discrete optimization technique applied in [A. P. Velo and G. A. Gazonas, <i>Int. J. Solids Structures</i> , 40 (2003), pp. 6417–6428]. For other layered designs, the optimality conditions are predicted heuristically using pattern recognition and the necessary conditions for the base angles and design parameters. Applications of these optimization results include design improvement in making a nonoptimal design optimal. They are also extended to non-Goupillaud-type layered media with integer layer length ratios. Our results are supported by numerical experiments and provide means to validate numerical optimization codes.					
15. SUBJECT TERMS Goupillaud-type layered media, wave propagation, palindromic polynomial, transient loading, shock wave, characteristic curves, periodic optimization, validation of numeric codes					
16. SECURITY CLASSIFICATION OF:			17. LIMITATION OF ABSTRACT UU	18. NUMBER OF PAGES 36	19a. NAME OF RESPONSIBLE PERSON George A. Gazonas
a. REPORT UNCLASSIFIED	b. ABSTRACT UNCLASSIFIED	c. THIS PAGE UNCLASSIFIED			19b. TELEPHONE NUMBER (Include area code) 410-306-0863

z -TRANSFORM METHODS FOR THE OPTIMAL DESIGN OF ONE-DIMENSIONAL LAYERED ELASTIC MEDIA*

ANI P. VELO[†], GEORGE A. GAZONAS[‡], AND TAKANOBU AMEYA[†]

Abstract. In this work, we develop a finite trigonometric series representation for the stress in a multilayered Goupillaud-type elastic strip subjected to transient Heaviside loading on one end while the other end is held fixed. This representation is achieved by means of the z -transform method and involves the so-called base angles. Generally, different layered designs could share the same set of base angles, and the more layers the design has, the more base angles are expected. Necessary conditions for the base angles and design parameters for any given design are described. As a result of the stress representation, we are able to identify optimal layered designs which provide the smallest stress amplitude. For two- and three-layered designs, for which the coefficients of the stress representation are easy to find, the optimization results are achieved using a custom-made discrete optimization technique applied in [A. P. Velo and G. A. Gazonas, *Int. J. Solids Structures*, 40 (2003), pp. 6417–6428]. For other layered designs, the optimality conditions are predicted heuristically using pattern recognition and the necessary conditions for the base angles and design parameters. Applications of these optimization results include design improvement in making a nonoptimal design optimal. They are also extended to non-Goupillaud-type layered media with integer layer length ratios. Our results are supported by numerical experiments and provide means to validate numerical optimization codes.

Key words. Goupillaud-type layered media, transient loading, wave propagation, shock wave, characteristic curves, palindromic polynomial, periodic optimization, validation of numerical codes

AMS subject classifications. 35A22, 35C05, 35L05, 35R05, 39A11, 49N20, 74P10

DOI. 10.1137/090751608

1. Introduction. In recent years, there has been a dramatic increase in the use of multilayered structures in technologies that include microelectromechanical system devices [2], [26], optical ratchets and etalons [20], [14], wide bandgap semiconductor devices [36], laser devices [3], [35], [21], and metamaterials for use as possible cloaking devices [8], to name a few. The optimal control of waves that propagate in such multilayered devices is governed by hyperbolic partial differential equations using distributed, boundary, interior pointwise, or other controls [24], [23], [22]. Despite the widespread use of multilayered structures in such diverse technological applications, exact analytical solutions to optimal design problems governed by the wave equation (hyperbolic systems) are virtually nonexistent in the literature. This is in part due to the fact that hyperbolic systems exhibit less regularity than parabolic systems [23]. Such solutions are especially useful for benchmarking or validating optimization codes which link formal nonlinear parameter estimation (optimization) algorithms with explicit finite element numerical codes. This paper extends the work reported in

*Received by the editors March 4, 2009; accepted for publication (in revised form) May 5, 2009; published electronically July 22, 2009. This research effort was partially sponsored by the Short Term Analysis Services (STAS) and Faculty Research and Engineering Program (FREPE), administered by the Battelle Memorial Institute in North Carolina for the U.S. Army Research Laboratory. This work was performed in part by an employee of the U.S. Government or under U.S. Government contract. The U.S. Government retains a nonexclusive, royalty-free license to publish or reproduce the published form of this contribution, or allow others to do so, for U.S. Government purposes. Copyright is owned by SIAM to the extent not limited by these rights.

<http://www.siam.org/journals/siap/70-3/75160.html>

[†]Department of Mathematics and Computer Science, University of San Diego, 5998 Alcalá Park, San Diego, CA 92110 (avelo@sandiego.edu, tameya@sandiego.edu).

[‡]Corresponding author. U.S. Army Research Laboratory, Weapons and Materials Research Directorate, Aberdeen Proving Ground, Aberdeen, MD 21005 (gazonas@arl.army.mil).

[34], where a lengthier discussion of prior work can be found; the interested reader can also consult the texts of [5], [27], and [4] for a geophysical perspective and analysis of wave propagation in multilayered media; a good review of transient wave propagation in layered media related to dispersion effects can be found in [33].

In this paper, we derive analytical optimal design solutions for stress wave propagation in a Goupillaud-type [12] elastic strip with up to five layers; Goupillaud-type layered elastic media have equal wave travel times in all layers. The elastic strip is subjected to a Heaviside step in stress loading at one end with the other end held fixed. Optimal designs are those designs which minimize the stress wave amplitude in all layers, for all time. Exact analytical expressions for the transiently propagating stress are found using the method of characteristics, which are generalized by writing them as layer recursion relationships. Symbolic algebra software such as Maple or Mathematica can be used to solve the layer recursion relationships in closed-form for a system of up to three layers. Desktop computer memory requirements are exceeded, however, for solutions in systems beyond the three-layer case, but the recurrence relations can be simplified by hand calculation using z -transform methods [15], [9], [25] and written in global matrix form [16]. Our global system of recursion relations requires only m -layer equations, whereas Knopoff's method requires $(2m + 1)$ -layer equations for scalar horizontally polarized shear waves [16], since we have summed up- and down-going wave amplitudes prior to deriving the layer recursion relationships. An excellent historical review can be found in [19], which compares Knopoff's global matrix method to the transfer matrix method [31], [13]. Our representation appears to be new to the field of wave propagation in multilayered elastic media, despite the long history of mathematical developments in the field and its connection to lattice filter theory [28].

We also observe that the z -domain system determinant forms a palindromic polynomial with real coefficients. The roots of this polynomial that lie on the unit circle and satisfy the optimality conditions relate to a countable and infinite set of optimal designs. A palindromic polynomial is equal to its reciprocal. A reciprocal characteristic determinant was also derived by [7] using the transfer matrix formalism [31], [13] for harmonic wave propagation in infinite layered elastic media. Reciprocal polynomials are finding increasing applications in dynamics [29] and in pure and applied mathematics [18], but we are not aware of any other work that relates them to the optimal design of problems governed by hyperbolic field equations. In section 2, we describe the general multilayered initial-boundary value problem that is to be solved and its reduction to global matrix form using z -transforms; the determinant of the global matrix is described by a palindromic polynomial in z . We assume that the roots of the polynomial lie on the unit circle and therefore are uniquely determined by their angle measure. In section 3, we describe two approaches to recovering necessary conditions that such angles and suitable design parameters must satisfy. We illustrate this using several examples. Optimal designs in multilayered elastic media subjected to Heaviside loading are illustrated in section 4, followed by applications in section 5.

2. Problem formulation, recursion relations, and solution using the z -transform method. We consider one-dimensional wave propagation in an isotropic multilayered elastic strip. As a generalization of [34], the strip is assumed to be of finite length L and consisting of elastic layers of arbitrary length L_1, L_2, \dots, L_m so that $L_1 + L_2 + \dots + L_m = L$. The strip is subjected to a Heaviside step in stress loading p at time $t = 0$ on one end and held fixed on the other end. Similar analysis may be extended to other initial and boundary conditions.

The density and elastic modulus along the strip are denoted by the piecewise constant functions $\rho(x)$ and $E(x)$, taking values ρ_i and E_i in the i th layer, respectively, $i = 1, 2, \dots, m$. In this work, we consider longitudinal elastic waves for a uniaxial strain state; however, our results are also valid for the case of uniaxial stress. The uniaxial strain elastic modulus E is related to the Young's modulus \bar{E} through the expression $E = \bar{E}(1 - \nu)/[(1 + \nu)(1 - 2\nu)]$, where ν is Poisson's ratio. Using the definition of the wave speed $c = (E/\rho)^{1/2}$, we relate to each layer the wave speed c_i for $i = 1, 2, \dots, m$. The characteristic impedance in the i th layer is given as a product of the material density ρ_i and wave speed c_i , while α_i , a design parameter, represents the impedance ratio between layer i and $i + 1$ for $i = 1, \dots, m - 1$. The transit time τ through the strip is given as

$$\tau = \frac{L_1}{c_1} + \frac{L_2}{c_2} + \dots + \frac{L_m}{c_m}.$$

Throughout this paper we assume a Goupillaud-type layered medium, which is a medium that ensures the same wave travel time through each layer,

$$(1) \quad \frac{L_1}{c_1} = \frac{L_2}{c_2} = \dots = \frac{L_m}{c_m} = \frac{\tau}{m}.$$

This problem can be easily converted to the case of m layers, all of equal length and wave speed of unity, by replacing the spatial variable x in the wave equation with the new variable $\xi = \int_0^x \frac{ds}{c(s)}$ and using condition (1). Here, $c \equiv c(s)$ is the piecewise constant wave speed function, taking values c_1, c_2, \dots, c_m in each layer, respectively. As a result, the wave equation becomes

$$\rho_i \frac{\partial^2 u}{\partial t^2} = \frac{1}{c_i} \frac{\partial}{\partial \xi} \left(\frac{E_i}{c_i} \frac{\partial u}{\partial \xi} \right) \quad \text{for } \frac{(i-1)\tau}{m} < \xi < \frac{i\tau}{m}, \quad i = 1, \dots, m.$$

Furthermore the wave speed becomes the same (unity) in each layer ($c = c_1 = c_2 = \dots = c_m = 1$) and the initial-boundary value problem becomes

$$(2) \quad \begin{cases} \frac{\partial^2 u(\xi, t)}{\partial t^2} = \frac{\partial^2 u(\xi, t)}{\partial \xi^2} & \text{for } \frac{(i-1)\tau}{m} < \xi < \frac{i\tau}{m}, \quad i = 1, \dots, m, \\ \sigma(0, t) = E_1 \frac{\partial u}{\partial \xi}(0, t) = pH(t), \quad u(\tau, t) = 0, \\ u(\xi, 0) = \frac{\partial u}{\partial t}(\xi, 0) = 0. \end{cases}$$

The functions $u(x, t)$ and $\sigma(x, t)$ represent the displacement and stress, respectively, at (x, t) , while $H(t)$ represents the Heaviside function. As a result, as done in [34] and without any loss of generality, the physical problem of the Goupillaud-type strip with layers of unequal lengths becomes equivalent to solving (2) for a Goupillaud-type strip of length $L = \tau$ and equal layer lengths of $\frac{\tau}{m}$, as shown in Figure 1. The time variable is represented on the vertical axis, where the (equal) wave travel time for each layer of the m layered strip in either direction is $\frac{\tau}{m}$. In Figure 1, the stress jump-discontinuities, which we call a shock wave, are propagated along the dashed characteristic lines of the wave equation, while the inner vertical solid lines represent the layer interfaces. Due to the zero initial conditions, the stress values below the first characteristic line segment with equation $t = \xi$ for $0 < \xi < \tau$ are zero. Above it, however, the intersection of characteristics with each other and the boundaries

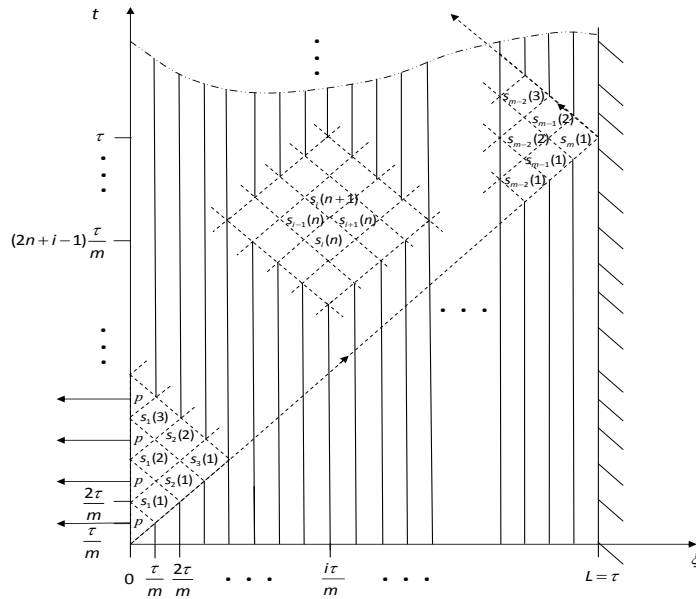


FIG. 1. Lagrangian diagram for an elastic strip made of m layers of equal wave travel time.

splits the region into square-box subregions. Due to the continuity of stress and displacement at each layer interface (discussed next), the stress value is constant in each square-box and is represented by $s_i(n)$, for $i = 1, 2, \dots, m$ and $n \geq 1$. Generally, if σ^+ represents the stress value ahead of the shock wave and σ^- represents the stress value behind the shock wave (see, e.g., [11]), then the stress jump is expressed as

$$(3) \quad \llbracket \sigma \rrbracket = \sigma^- - \sigma^+,$$

and $\llbracket \sigma \rrbracket = 0$ for spatially continuous waves. Furthermore, when the shock wave propagates from one layer to the next, we have that

$$(4) \quad \llbracket \sigma \rrbracket_T = \frac{2}{1 + \alpha} \llbracket \sigma \rrbracket_I \quad \text{and} \quad \llbracket \sigma \rrbracket_R = \frac{1 - \alpha}{1 + \alpha} \llbracket \sigma \rrbracket_I.$$

The subscripts refer to I (incident), T (transmitted), and R (reflected) wave. The impedance ratio between the first and the second layers is represented by α . The coefficients in (4) represent the reflection and transmission coefficients for the stress wave, derived from the continuity conditions of the stress and displacement at the layer interface; see [32]. Due to reflections at the layer interfaces and boundary, the stress waves travel in both directions. These superposing waves interfere in accordance with the principle of superposition. For an m -layered strip, due to the equal wave travel time for each layer, the left and right propagating waves arrive/split at the same time at the layer interfaces.

After applying (3), (4) and the principle of superposition at each layer interface and boundary, we generalize the results for the two-layered strip studied in [34] and derive the following system of coupled first order difference equations relating the

stress terms in an m -layered strip:

$$(5) \quad \begin{cases} s_1(n+1) = -s_1(n) + \frac{2\alpha_1}{1+\alpha_1}s_2(n) + \frac{2}{1+\alpha_1}p, \\ s_2(n+1) = -s_2(n) + \frac{2\alpha_2}{1+\alpha_2}s_3(n) + \frac{2}{1+\alpha_2}s_1(n+1), \\ \dots \\ s_i(n+1) = -s_i(n) + \frac{2\alpha_i}{1+\alpha_i}s_{i+1}(n) + \frac{2}{1+\alpha_i}s_{i-1}(n+1), \\ \dots \\ s_{m-1}(n+1) = -s_{m-1}(n) + \frac{2\alpha_{m-1}}{1+\alpha_{m-1}}s_m(n) + \frac{2}{1+\alpha_{m-1}}s_{m-2}(n+1), \\ s_m(n+1) = -s_m(n) + 2s_{m-1}(n+1). \end{cases}$$

Here $n \geq 0$ is a suitable time index, while $s_i(0) = 0$ for all $1 \leq i \leq m$ expresses the zero-stress initial conditions. The nonnegative integer values of $n \geq 0$ are used to count the stress terms over time, as shown in Figure 1. The stress value is constant within each box in Figure 1. The center of the square-box with the stress value $s_i(n)$ in Figure 1 is the point with coordinates $\xi = i\frac{\pi}{m}$ and $t = (2n+i-1)\frac{\pi}{m}$. As mentioned before, the impedance in each layer is given as a product of the material density ρ and wave speed $c = 1$, while α_i represents the impedance ratio between layer i and $i + 1$, for $i = 1, \dots, m - 1$.

Notice that in Figure 1 the values of the stress in each layer alternate between the terms of two sequences. Starting from the left, the stress values in layer 1 are $p, s_1(1), p, s_1(2), p, s_1(3)$, and so on. Similarly, the first few stress values in layer 2 are $s_1(1), s_2(1), s_1(2), s_2(2), s_1(3), s_2(3)$. This is illustrated later with the graphs in section 4. When positioned in the middle of the i th or $(i + 1)$ th layer of an m -layered strip, the time interval at which $s_i(n)$ is reached is $\frac{4n+2i-3}{2m} < t < \frac{4n+2i-1}{2m}$, as depicted in Figures 2, 3, 7, and 8 below. Here $n \geq 1$ and $i = 0, 1, 2, \dots, m$. When $i = 0$, $s_0(n) = p$ represents the constant p -sequence taking values on the first layer only, while when $i = m$, $s_m(n)$ represents the general term of the last sequence taking values on the m th layer only.

As shown later, the system (5) of difference equations can be solved easily for a small number of layers, $1 \leq m \leq 3$, but it becomes quite involved for $m \geq 4$. Applying the z -transform to the system of difference equations (5) allows us to convert it into an $m \times m$ linear algebraic system (6), which is easier to solve. Then, we use the inverse z -transform to recover the formulas for the stress terms $s_i(n)$, for $i = 1, \dots, m$ and $n \geq 0$. As a result we provide a general representation (14)–(15) for the stress in terms of the so-called base angles.

Indeed, due to the zero-stress initial conditions $s_i(0) = 0$ for all $1 \leq i \leq m$, the z -transform of $s_i(n + 1)$ becomes

$$Z(s_i(n + 1)) = zS_i(z) - zs_i(0) = zS_i(z),$$

where $S_i(z)$ is the z -transform of $s_i(n)$. Thus the z -transform¹ of (5) is expressed as

$$(6) \quad \begin{cases} zS_1(z) = -S_1(z) + \frac{2\alpha_1}{1+\alpha_1}S_2(z) + \frac{2}{1+\alpha_1}p \cdot \frac{z}{z-1}, \\ zS_2(z) = -S_2(z) + \frac{2\alpha_2}{1+\alpha_2}S_3(z) + \frac{2}{1+\alpha_2}zS_1(z), \\ \dots \\ zS_i(z) = -S_i(z) + \frac{2\alpha_i}{1+\alpha_i}S_{i+1}(z) + \frac{2}{1+\alpha_i}zS_{i-1}(z), \\ \dots \\ zS_{m-1}(z) = -S_{m-1}(z) + \frac{2\alpha_{m-1}}{1+\alpha_{m-1}}S_m(z) + \frac{2}{1+\alpha_{m-1}}zS_{m-2}(z), \\ zS_m(z) = -S_m(z) + 2zS_{m-1}(z). \end{cases}$$

¹The definition for the z -transform of $g(n)$, $n \geq 0$, is $Z(g(n)) = G(z) = \sum_{n=0}^{\infty} g(n)z^{-n}$ for $|z| > R$ in the complex plane.

After reorganizing the terms in (6), we write this linear system in the matrix-vector form as

$$(7) \quad A_m \vec{x}_m = \vec{b}_m,$$

where A_m is a tridiagonal matrix given as

$$(8) \quad A_m = \begin{bmatrix} z+1 & -\eta_1\alpha_1 & 0 & \cdots & 0 & 0 & 0 & 0 \\ -\eta_2z & z+1 & -\eta_2\alpha_2 & 0 & \cdots & 0 & 0 & 0 \\ 0 & -\eta_3z & z+1 & -\eta_3\alpha_3 & 0 & \cdots & 0 & 0 \\ \vdots & \vdots \\ 0 & 0 & 0 & \cdots & 0 & -\eta_{m-1}z & z+1 & -\eta_{m-1}\alpha_{m-1} \\ 0 & 0 & 0 & \cdots & 0 & 0 & -\eta_mz & z+1 \end{bmatrix}_{m \times m},$$

while

$$\vec{x}_m = \begin{bmatrix} S_1(z) \\ S_2(z) \\ \vdots \\ S_m(z) \end{bmatrix}_{m \times 1}, \quad \vec{b}_m = \begin{bmatrix} \eta_1 p \cdot \frac{z}{z-1} \\ 0 \\ \vdots \\ 0 \end{bmatrix}_{m \times 1}, \quad \eta_i = \frac{2}{1 + \alpha_i} \text{ for } i = 1, \dots, m-1, \eta_m = 2.$$

Due to the sparseness of \vec{b}_m , the solution of the linear system (7) is

$$(9) \quad \vec{x}_m = A_m^{-1} \vec{b}_m = \frac{\eta_1 p z}{(z-1)|A_m|} \begin{bmatrix} (-1)^{1+1}|A_{1,1}| \\ (-1)^{1+2}|A_{1,2}| \\ \vdots \\ (-1)^{1+m}|A_{1,m}| \end{bmatrix} = \frac{\eta_1 p z}{(z-1)|A_m|} \begin{bmatrix} |A_{1,1}| \\ -|A_{1,2}| \\ \vdots \\ (-1)^{1+m}|A_{1,m}| \end{bmatrix}.$$

Here $|A_m|$ is the determinant of A_m , $A_{1,j}$ for $j = 1, \dots, m$ are minors of A_m , and $|A_{1,j}|$ are their corresponding determinants.

One can derive by induction that the determinant $|A_m|$ is a palindromic polynomial with real coefficients; i.e., the coefficients in front of z^{m-j} and z^j are real and equal to each other for $j = 0, \dots, m$, and $m \geq 1$. Furthermore, the algebraic structure of the palindromic polynomials of even degree in (10) allows the inverse of a root to

also be a root; i.e., if r is a root, then $\frac{1}{r}$ is also a root. Thus we have

(10)

$$|A_m| = \begin{cases} z^m + a_{m,1}z^{m-1} + a_{m,2}z^{m-2} + \dots + a_{m,\frac{m}{2}-1}z^{\frac{m}{2}+1} + a_{m,\frac{m}{2}}z^{\frac{m}{2}} \\ + a_{m,\frac{m}{2}-1}z^{\frac{m}{2}-1} + \dots + a_{m,2}z^2 + a_{m,1}z + 1 & \text{for } m \text{ even,} \\ (z+1)[z^{m-1} + b_{m,1}z^{m-2} + \dots + b_{m,\frac{m-1}{2}-1}z^{\frac{m-1}{2}+1} + b_{m,\frac{m-1}{2}}z^{\frac{m-1}{2}} \\ + b_{m,\frac{m-1}{2}-1}z^{\frac{m-1}{2}-1} + \dots + b_{m,2}z^2 + b_{m,1}z + 1] & \text{for } m \text{ odd.} \end{cases}$$

As a result we obtain

$$(11) \quad |A_m| = \begin{cases} \prod_{k=1}^{\lfloor \frac{m}{2} \rfloor} [z^2 - (z_k + z_k^{-1})z + 1] & \text{for } m \text{ even,} \\ (z+1) \prod_{k=1}^{\lfloor \frac{m}{2} \rfloor} [z^2 - (z_k + z_k^{-1})z + 1] & \text{for } m \text{ odd.} \end{cases}$$

The assumption that all the roots are on the unit circle implies that $z_k = e^{i\theta_k} = \cos \theta_k + i \sin \theta_k$ and $z_k^{-1} = e^{-i\theta_k} = \cos \theta_k - i \sin \theta_k$ for $1 \leq k \leq \lfloor \frac{m}{2} \rfloor$ and $i = \sqrt{-1}$. This guarantees real coefficients for the polynomials in (11). This assumption is motivated by the fact that the homogeneous design solutions for the m -layer case all lie on the unit circle (see subsection 4.4), and by the fact that all (optimal) design solutions for the two- and three-layer cases, which are independently derived in subsections 2.1–2.2, also lie on the unit circle. The work of [30] seems to be in favor of this argument as well. After substituting the expression

$$z_k + z_k^{-1} = z_k + \bar{z}_k = 2 \cos \theta_k$$

back into (11), we have a newly factored representation for the polynomial(s) with real coefficients $|A_m|$ in terms of the angles $\theta_1, \theta_2, \dots, \theta_{\lfloor \frac{m}{2} \rfloor}$ as shown below:

$$(12) \quad |A_m| = \begin{cases} \prod_{k=1}^{\lfloor \frac{m}{2} \rfloor} [z^2 - 2 \cos(\theta_k)z + 1] & \text{for } m \text{ even,} \\ (z+1) \prod_{k=1}^{\lfloor \frac{m}{2} \rfloor} [z^2 - 2 \cos(\theta_k)z + 1] & \text{for } m \text{ odd.} \end{cases}$$

Based on the factorization of the determinant $|A_m|$, for any m -layered design, when there are m distinct roots on the unit circle there are m distinct angles: $\{\pm\theta_k\}_{k=1}^{\frac{m}{2}}$ when m is even, and $\theta_0 = \pi, \{\pm\theta_k\}_{k=1}^{\lfloor \frac{m}{2} \rfloor}$ when m is odd. From now on, for an m -layered design, the $\lfloor \frac{m}{2} \rfloor$ essential angles $0 < \theta_k < \pi$ for $k = 1, \dots, \lfloor \frac{m}{2} \rfloor$ will be called the base angles. Furthermore, since the degree of $|A_m|$ is m and the degree of $|A_{1,i}|$ is $m - 1$, for $i = 1, 2, \dots, m$, the substitution of (12) into (9) allows the following expansion of the components $\vec{x}_m(i)$ of \vec{x}_m into partial fractions:

$$\vec{x}_m(i) = \left[\frac{(-1)^i \eta_1 |A_{1,i}|}{|A_m|(z-1)} \right] \cdot pz = \left[\frac{a_{i,0}}{z-1} + \frac{b_{i,0}}{z+1} + \sum_{k=1}^{\lfloor \frac{m}{2} \rfloor} \frac{a_{i,k}^* \cdot z + b_{i,k}^*}{z^2 - 2 \cos(\theta_k)z + 1} \right] \cdot pz,$$

where the coefficients $b_{i,0} = 0$ for even m and $i = 1, 2, \dots, m$.

Assuming that the so-called base angles $0 < \theta_k < \pi$ for $1 \leq k \leq \lfloor \frac{m}{2} \rfloor$ are distinct and therefore correspond to distinct roots with $\sin \theta_k \neq 0$, for all $k = 1, \dots, \lfloor \frac{m}{2} \rfloor$, the following choices for the coefficients,

$$a_{i,k} = a_{i,k}^*, \quad b_{i,k} = \frac{a_{i,k}^* \cos \theta_k + b_{i,k}^*}{\sin \theta_k},$$

allow the expansion of each component of the solution vector to be of the form (13)

$$\vec{x}_m(i) = \left[\frac{a_{i,0} \cdot z}{z-1} + \frac{b_{i,0} \cdot z}{z+1} + \sum_{k=1}^{\lfloor \frac{m}{2} \rfloor} \left(\frac{a_{i,k} \cdot z(z - \cos \theta_k)}{z^2 - 2 \cos(\theta_k)z + 1} + \frac{b_{i,k} \cdot z \sin \theta_k}{z^2 - 2 \cos(\theta_k)z + 1} \right) \right] \cdot p.$$

In this paper we consider only stress solutions with their corresponding z -transforms expressed by (13). Finally, after applying the inverse z -transform to (13), we obtain solutions of (5) in the form of finite trigonometric series,

$$(14) \quad s_i(n) = \left[a_{i,0} + b_{i,0}(-1)^n + \sum_{k=1}^{\lfloor \frac{m}{2} \rfloor} a_{i,k} \cos(n\theta_k) + b_{i,k} \sin(n\theta_k) \right] \cdot p,$$

for $i = 1, 2, \dots, m$, $n \geq 0$, and as it follows from (5),

$$(15) \quad \begin{cases} s_i(1) = \frac{2^i}{\prod_{j=1}^i (1+\alpha_j)} p & \text{for } i = 1, \dots, m-1, \\ s_m(1) = \frac{2^m}{\prod_{j=1}^{(m-1)} (1+\alpha_j)} p. \end{cases}$$

As before, $b_{i,0} = 0$ for m even and $i = 1, \dots, m$. For a given design, the stress solutions in (14) are bounded. The terms of the (trigonometric) sum that multiplies p in (14) are expected to depend only on the impedance ratios $\alpha_1, \alpha_2, \dots, \alpha_{m-1}$, as these are the only design parameters inherited from (8). As shown in the next sections, fewer design parameters which are combinations of the impedance ratios become relevant for the base angles and stress optimization in the m -layer case. Such design parameters for an m -layered strip will be $\chi_{m-1} = \prod_{j=1}^{m-1} (1+\alpha_j)$ for $m \geq 2$ and Γ_{m-1} for $m = 4, 5$, defined later.

In summary, the stress terms for the m -layered Goupillaud-type media are expressed in the form of finite trigonometric series that involve multiples of $\lfloor \frac{m}{2} \rfloor$ base angles denoted by $\theta_1, \theta_2, \dots, \theta_{\lfloor \frac{m}{2} \rfloor}$. This also implies that the more layers the design has, the more base angles are expected. According to the formula (14), each stress term is a factor of the loading parameter p . This means that the value of each stress term will increase/decrease as many times as the applied loading. These findings match with the results given in the later subsections for the two- and three-layered media, where only one base angle per design appears. Special values of this angle generate optimal designs. However, when $m \geq 4$, more than one base angle is expected to appear, and the process of explicitly finding the coefficients of the trigonometric series in (14) becomes more complicated.

From (14) one can easily notice that if one stress sequence with nonzero coefficients in front of the sine or cosine of each θ_k , $k = 1, \dots, \lfloor \frac{m}{2} \rfloor$, is periodic, then all the stress sequences derived for that design are periodic. The common period T is a positive integer which satisfies the relation $T\theta_k = 2\pi j_k$, for $k = 1, 2, \dots, \lfloor \frac{m}{2} \rfloor$, where j_k take positive integer values in increasing order. When $j_1 = 1$, the corresponding base angle $\theta_1 = 2\pi/T$ represents the circular frequency. In addition, for an odd number of layers, the presence of $(-1)^n$ in the stress formulas implies that the period T is an even positive integer. As seen later in section 4, periodic stress sequences are of special importance, as they characterize optimal designs.

2.1. The two-layer case: Stress representation and periodicity. For the two-layered strip with $m = 2$, one may solve system (5) of the difference equations

directly or by means of symbolic algebra software such as Maple or Mathematica. As a result, the stress terms can be represented in a form consistent with that shown in (14), where the z -transform was used together with the assumption that the roots in the z -space lie on the unit circle. The stress terms are expressed as follows:

$$(16) \quad \begin{cases} s_1(n) = [1 - \cos n\theta_1] \cdot p, \\ s_2(n) = [1 - \cos n\theta_1 - \frac{1}{\sqrt{\chi_1-1}} \sin n\theta_1] \cdot p, \end{cases} \quad \text{for } n \geq 1.$$

After a few mathematical manipulations one can also verify that these results are the same as those given in [34]. Here the design parameter χ_1 is given by $\chi_1 = (\alpha_1 + 1)$, while θ_1 represents the (only) base angle. For $\chi_1 > 2$ and $0 < \theta_1 < \frac{\pi}{2}$, we have that $\theta_1 = \arctan(\frac{2\sqrt{\chi_1-1}}{\chi_1-2})$, and

$$(17) \quad \boxed{\chi_1 = \frac{2}{1 - \cos\theta_1} \text{ or, equivalently, } \cos\theta_1 = \frac{\chi_1 - 2}{\chi_1} = \frac{\alpha_1 - 1}{\alpha_1 + 1}.}$$

As seen later in section 4, $\chi_1 > 2$ is the reduced interval considered for stress optimization, and the optimal designs are characterized by periodic solutions for the stress sequences $s_1(n)$ and $s_2(n)$, $n \geq 0$. Representation (16) is convenient for deriving some key properties of such periodic solutions. We determine the (common) period T using the fact that the sine and cosine functions are periodic with period 2π . Thus we have $\cos[(n + T)\theta] = \cos n\theta$, which implies that $T\theta = 2\pi$. Considering the fact that the common period T is some positive integer, the stress sequences are periodic with respect to $n \geq 0$ iff the base angle is expressed as

$$\theta_1 = \frac{2\pi}{T}, \quad \text{where } T \text{ is a positive integer.}$$

The base angle θ_1 represents the circular frequency. As a result, for a given two-layered design, if one sequence of the stress terms is periodic with respect to n , so is the other stress sequence. When periodic, both sequences $\{s_j(n)\}$, $n \geq 0$, $j = 1, 2$, share a common period and frequency. Each of the periodic stress solutions/sequences can be represented in the form $\delta \sin(n\theta + \phi) + \gamma$ and are therefore expected to have a sinusoidal shape with $T \geq 2m = 4$. Here δ , ϕ , and γ are constants and ϕ represents the phase at $n = 0$.

2.2. The three-layer case: Stress representation and periodicity. Similar to the two-layered strip, one may solve system (5) for the three-layer case with $m = 3$ and represent the stress terms in a form consistent with that shown in (14):

$$(18) \quad \begin{cases} s_1(n) = \left[1 - \frac{\alpha_2}{\chi_2-1} (-1)^n - \frac{\alpha_1+\alpha_1\alpha_2}{\chi_2-1} \cos n\theta_1 \right] \cdot p, \\ s_2(n) = \left[1 - \cos n\theta_1 + \frac{1}{\sqrt{\chi_2-1}} \sin n\theta_1 \right] \cdot p, \\ s_3(n) = \left[1 - \frac{1}{\chi_2-1} (-1)^n - \frac{\chi_2-2}{\chi_2-1} \cos n\theta_1 + \frac{2}{\sqrt{\chi_2-1}} \sin n\theta_1 \right] \cdot p, \end{cases} \quad \text{for } n \geq 1.$$

Here the design parameter χ_2 is given by $\chi_2 = (\alpha_1 + 1)(\alpha_2 + 1) > 1$, while θ_1 represents the (only) base angle. As before, for $\chi_2 > 2$ and $0 < \theta_1 < \frac{\pi}{2}$, we have that

$\theta_1 = \arctan\left(\frac{2\sqrt{\chi_2-1}}{\chi_2-2}\right)$. As a result,

$$(19) \quad \boxed{\chi_2 = \frac{2}{1 - \cos\theta_1} \quad \text{or, equivalently,} \quad \cos\theta_1 = \frac{\chi_2 - 2}{\chi_2}.}$$

Relation (19) suggests that different designs with the same value of χ_2 share the same base angle θ_1 . In other words, different layered designs can share the same set of base angles.

As seen later in section 4 and similar to the two-layer case, periodic solutions for the stress sequences $s_1(n)$, $s_2(n)$, and $s_3(n)$, $n \geq 0$, characterize three-layered optimal designs. The presence of the term $(-1)^n$ in the stress formulas for an odd number of layers implies that when $m = 3$ the common period T must be an even number, i.e., that $T = 2l$, for $l \geq 3$. As in the two-layer case, the stress sequences are periodic with respect to $n \geq 0$ iff the base angle is expressed as

$$\theta_1 = \frac{2\pi}{T}, \quad \text{where } T \text{ is a positive even integer.}$$

The base angle θ_1 represents the circular frequency. For a given three-layered design, if one sequence of the stress terms is periodic with respect to n , so are the other two. As seen later in section 4, when periodic, all sequences $\{s_j(n)\}$, $n \geq 0$, $j = 1, 2, 3$, share a common period and frequency.

3. Necessary conditions for the base angles and design parameters. As discussed in the previous section, an m -layered Goupillaud-type design has $\lfloor \frac{m}{2} \rfloor$ distinct base angles, $0 < \theta_1, \theta_2, \dots, \theta_{\lfloor \frac{m}{2} \rfloor} < \pi$. In this section we describe two approaches that reveal necessary conditions which the base angles and suitable design parameters must satisfy for any given design.

3.1. Approach 1: Testing the stress representation. The stress representation formulas (14) must satisfy the recursive relations (5) for all $n \geq 0$. Ultimately, this test will reveal condition (25) that each base angle has to satisfy. Developing condition (25) will allow us to relate each base angle with suitable design parameters.

Indeed, after substituting back the stress expressions (14) into (5), regrouping the terms, and using the trigonometric sum formulas

$$\cos(n + 1)\theta = \cos n\theta \cos \theta - \sin n\theta \sin \theta$$

and

$$\sin(n + 1)\theta = \sin n\theta \cos \theta + \cos n\theta \sin \theta,$$

we obtain the equations that follow.

The first recursive relation in (5) becomes

$$(20) \quad \begin{aligned} & 2 \left[a_{1,0} - \frac{\alpha_1}{1 + \alpha_1} \cdot a_{2,0} - \frac{1}{1 + \alpha_1} \right] - \frac{2\alpha_1}{1 + \alpha_1} (-1)^n \cdot b_{2,0} \\ & + \sum_{k=1}^{\lfloor \frac{m}{2} \rfloor} \left[(\cos \theta_k + 1) \cdot a_{1,k} + \sin \theta_k \cdot b_{1,k} - \frac{2\alpha_1}{1 + \alpha_1} \cdot a_{2,k} \right] \cdot \cos n\theta_k \\ & + \sum_{k=1}^{\lfloor \frac{m}{2} \rfloor} \left[-\sin \theta_k \cdot a_{1,k} + (1 + \cos \theta_k) \cdot b_{1,k} - \frac{2\alpha_1}{1 + \alpha_1} \cdot b_{2,k} \right] \cdot \sin n\theta_k = 0. \end{aligned}$$

The i th recursive relation in (5), for $i = 2, 3, \dots, m - 1$, becomes

$$\begin{aligned}
 & 2 \left[-\frac{1}{1 + \alpha_i} \cdot a_{i-1,0} + a_{i,0} - \frac{\alpha_i}{1 + \alpha_i} \cdot a_{i+1,0} \right] + \frac{2(-1)^n}{1 + \alpha_i} [b_{i-1,0} - \alpha_i \cdot b_{i+1,0}] \\
 & + \sum_{k=1}^{\lfloor \frac{m}{2} \rfloor} \left[-\frac{2}{1 + \alpha_i} \cos \theta_k \cdot a_{i-1,k} - \frac{2}{1 + \alpha_i} \sin \theta_k \cdot b_{i-1,k} \right. \\
 (21) \quad & \left. + (\cos \theta_k + 1) \cdot a_{i,k} + \sin \theta_k \cdot b_{i,k} - \frac{2\alpha_i}{1 + \alpha_i} \cdot a_{i+1,k} \right] \cdot \cos n\theta_k \\
 & + \sum_{k=1}^{\lfloor \frac{m}{2} \rfloor} \left[-\frac{2}{1 + \alpha_i} \sin \theta_k \cdot a_{i-1,k} - \frac{2}{1 + \alpha_i} \cos \theta_k \cdot b_{i-1,k} - \sin \theta_k \cdot a_{i,k} \right. \\
 & \left. + (1 + \cos \theta_k) \cdot b_{i,k} - \frac{2\alpha_1}{1 + \alpha_1} \cdot b_{i+1,k} \right] \cdot \sin n\theta_k = 0,
 \end{aligned}$$

and the last recursive relation in (5) becomes

$$\begin{aligned}
 & 2[-a_{m-1,0} + a_{m,0}] + 2(-1)^n \cdot b_{m-1,0} \\
 & + \sum_{k=1}^{\lfloor \frac{m}{2} \rfloor} [-2 \cos \theta_k \cdot a_{m-1,k} - 2 \sin \theta_k \cdot b_{m-1,k} \\
 (22) \quad & + (\cos \theta_k + 1) \cdot a_{m,k} + \sin \theta_k \cdot b_{m,k}] \cdot \cos n\theta_k \\
 & + \sum_{k=1}^{\lfloor \frac{m}{2} \rfloor} [2 \sin \theta_k \cdot a_{m-1,k} - 2 \cos \theta_k \cdot b_{m-1,k} - \sin \theta_k \cdot a_{m,k} \\
 & + (1 + \cos \theta_k) \cdot b_{m,k}] \cdot \sin n\theta_k = 0.
 \end{aligned}$$

Considering the fact that the sums above must equal zero for all values of $n \geq 0$ and for all the base angles $\theta_1, \theta_2, \dots, \theta_{\lfloor \frac{m}{2} \rfloor}$, we require that the combination of the free terms, the terms multiplying $\cos n\theta_k$, and $\sin n\theta_k$ equal zero separately. One can easily check that the coefficients in (16) and (18) for the two- and three-layer cases, respectively, satisfy these proposed conditions. The zero-conditions involving the terms multiplying $\cos n\theta_k$ and $\sin n\theta_k$ imply that for any base angle $\theta_k, k = 1, \dots, \lfloor \frac{m}{2} \rfloor$, represented by θ below, we have

$$(23) \quad D_m \vec{v} = \vec{0},$$

where

$$D_m = \begin{bmatrix} F & B_1 & 0 & \dots & & & \dots & 0 \\ C_2 & F & B_2 & 0 & \dots & & \dots & 0 \\ 0 & C_3 & F & B_3 & 0 & \dots & \dots & 0 \\ & \ddots & & \ddots & \ddots & & & \\ 0 & \dots & & \dots & 0 & C_i & F & B_i & 0 & \dots & \dots & 0 \\ & & & & & \ddots & & \ddots & \ddots & & & 0 \\ 0 & \dots & & & & & \dots & 0 & C_{m-1} & F & B_{m-1} & \\ 0 & \dots & & & & & \dots & 0 & C_m & F & & \end{bmatrix}_{2m \times 2m},$$

$$(24) \quad \vec{v} = \begin{bmatrix} a_{k,1} \\ b_{k,1} \\ a_{k,2} \\ b_{k,2} \\ a_{k,3} \\ b_{k,3} \\ \vdots \\ a_{k,i} \\ b_{k,i} \\ \vdots \\ a_{k,m-1} \\ b_{k,m-1} \\ a_{k,m} \\ b_{k,m} \end{bmatrix}_{2m \times 1}, \quad \begin{aligned} F &= \begin{bmatrix} 1 + \cos \theta & \sin \theta \\ -\sin \theta & (1 + \cos \theta) \end{bmatrix}_{2 \times 2}, \quad |F| = 2(1 + \cos \theta), \\ B_i &= \begin{bmatrix} -\frac{2\alpha_i}{1+\alpha_i} & 0 \\ 0 & -\frac{2\alpha_i}{1+\alpha_i} \end{bmatrix}_{2 \times 2} = \frac{4\alpha_i^2}{(1 + \alpha_i)^2} I, \quad |B_i| = \frac{4\alpha_i^2}{(1 + \alpha_i)^2}, \\ C_i &= \begin{bmatrix} -\frac{2}{1+\alpha_i} \cos \theta & -\frac{2}{1+\alpha_i} \sin \theta \\ \frac{2}{1+\alpha_i} \sin \theta & -\frac{2}{1+\alpha_i} \cos \theta \end{bmatrix}_{2 \times 2} = \frac{4}{(1 + \alpha_i)^2} R^T, \\ |C_i| &= \frac{4}{(1 + \alpha_i)^2}, \quad 1 \leq i \leq m - 1, \\ C_m &= \begin{bmatrix} -2 \cos \theta & -2 \sin \theta \\ 2 \sin \theta & -2 \cos \theta \end{bmatrix}_{2 \times 2} = 4R^T, \quad |C_m| = 4. \end{aligned}$$

Here I represents the 2×2 identity matrix, while R^T represents the transpose of the rotation matrix $R = \begin{bmatrix} \cos \theta & -\sin \theta \\ \sin \theta & \cos \theta \end{bmatrix}$. The determinant of the matrix D_m for $m = 2, 3$ can be easily calculated using Laplace's theorem.

The nonzero vector \vec{v} of stress coefficients in (23)–(24) demands that

$$(25) \quad |D_m| = 0,$$

a condition which reveals a necessary relationship of each base angle with suitable design parameters. Below we demonstrate how this approach works for the three-layer case with $m = 3$. Indeed, condition (25) implies that $|D_3| = 0$ or equivalently that

$$\cos(\theta_1) = -1 \quad \text{or} \quad [\chi_2 \cos \theta_1 - (\chi_2 - 2)]^2 = 0.$$

Besides $\theta_1 = \pi$, we also derive the double root

$$\cos \theta_1 = \frac{\chi_2 - 2}{\chi_2},$$

previously obtained in (19) from the known stress solutions.

In conclusion, (25) with D_m described in (24) displays necessary conditions that each base angle and relevant design parameter(s) must satisfy for the m -layer case. Solving (25) for large values of m can be a computational challenge. This approach does not directly display the relations among the base angles except for the fact that they all satisfy the same condition (25).

3.2. Approach 2: Relating the coefficients of the palindromic polynomials with their roots in the z-space. The same necessary conditions for the base angles and design parameters discussed in the previous subsection can also be derived by relating the coefficients of the palindromic polynomial $|A_m|$ with its roots; see (10), (11), and (12). Below we illustrate how this approach works using a few cases.

The three-layer case ($m = 3$). Based on (10), (11), and (12) there are two different ways to represent the determinant $|A_3|$,

$$|A_3| = (z + 1) \cdot \left[z^2 - \frac{2(\chi_2 - 2)}{\chi_2} z + 1 \right] \quad (\text{see (45)})$$

and

$$|A_3| = (z + 1)(z - e^{i\theta_1})(z - e^{-i\theta_1}) = (z + 1)(z^2 - 2 \cos \theta_1 z + 1).$$

After matching the coefficients in front of equal powers of z or using Vieta's theorem, we obtain that

$$\cos \theta_1 = \frac{\chi_2 - 2}{\chi_2}.$$

This is the same necessary condition derived in the previous subsection as well as in (19) from the known stress solutions.

The four-layer case ($m = 4$). Similarly, the two different representations of the determinant

$$\begin{aligned} |A_4| = z^4 - \frac{4(-1 + \alpha_1 \alpha_3)}{(1 + \alpha_1)(1 + \alpha_2)(1 + \alpha_3)} z^3 + 2 \left(-1 + \frac{4(1 + \alpha_1 \alpha_3)}{(1 + \alpha_1)(1 + \alpha_2)(1 + \alpha_3)} \right) z^2 \\ - \frac{4(-1 + \alpha_1 \alpha_3)}{(1 + \alpha_1)(1 + \alpha_2)(1 + \alpha_3)} z + 1 \quad (\text{see (45)}) \end{aligned}$$

and

$$\begin{aligned} |A_4| &= (z - e^{i\theta_1})(z - e^{-i\theta_1})(z + e^{i\theta_2})(z - e^{i\theta_2}) \\ &= (z^2 - 2z \cos \theta_1 + 1)(z^2 - 2z \cos \theta_2 + 1) \\ &= z^4 - 2(\cos \theta_1 + \cos \theta_2)z^3 + 2(1 + 2 \cos \theta_1 \cos \theta_2)z^2 - 2(\cos \theta_1 + \cos \theta_2)z + 1 \end{aligned}$$

imply the following necessary conditions between the cosines of the two base angles θ_1 , θ_2 and design parameters χ_3 and Γ_3 :

$$(26) \quad \begin{cases} \cos \theta_1 + \cos \theta_2 = \frac{2\Gamma_3}{\chi_3}, \\ \cos \theta_1 \cdot \cos \theta_2 = \frac{2\Gamma_3 - \chi_3 + 4}{\chi_3}. \end{cases}$$

Here $\chi_3 = (1 + \alpha_1)(1 + \alpha_2)(1 + \alpha_3)$ and $\Gamma_3 = (\alpha_1 \alpha_3 - 1)$ represent the only two relevant design parameters. Relations (26) also imply that $\cos \theta_{1,2}$ satisfy the quadratic equation

$$(27) \quad \chi_3 \cos^2 \theta - 2\Gamma_3 \cos \theta + (2\Gamma_3 - \chi_3 + 4) = 0.$$

For the special case of a homogeneous design ($\alpha_1 = \alpha_2 = \alpha_3 = 1$) we have that $\chi_3 = 8$ and $\Gamma_3 = 0$. Substituting these values into the quadratic equation (27), we find that the corresponding base angles $0 < \theta_1 = \frac{\pi}{4}, \theta_2 = \frac{3\pi}{4} < \pi$, satisfy $2\cos(\theta) = z + \frac{1}{z} = \pm \frac{2}{\sqrt{2}}$. This matches with the regular distribution patterns for the optimal angles discussed in subsection 4.4. A mapping that takes the unit circle to the real interval $[-2, 2]$, which expresses the range of values of $2\cos(\theta)$, is discussed in [6]. This is accompanied by a size reduction from a fourth order polynomial to a quadratic. In our case, the fourth order polynomial $|A_4|$ in z (see (45)) is replaced by the quadratic polynomial (27) for $\cos \theta$. Notice that although a four-layer design has three impedance ratios, based on (26) there are only two relevant design parameters χ_3 and Γ_3 obtained as special combinations of these impedance ratios. The number (two) of the relevant design parameters appears to equal the number of the base angles.

The five-layer case ($m = 5$). Similar to the four-layer case, one may obtain the following relations between the cosines of the two base angles θ_1, θ_2 and design parameters χ_4 and Γ_4 :

$$(28) \quad \begin{cases} \cos \theta_1 + \cos \theta_2 = \frac{2\Gamma_4}{\chi_4}, \\ \cos \theta_1 \cdot \cos \theta_2 = \frac{2\Gamma_4 - \chi_4 + 4}{\chi_4}. \end{cases}$$

Here $\chi_4 = (1 + \alpha_1)(1 + \alpha_2)(1 + \alpha_3)(1 + \alpha_4)$ and $\Gamma_4 = (\alpha_1\alpha_3\alpha_4 + \alpha_1\alpha_2\alpha_4 + \alpha_1\alpha_4 + \alpha_2\alpha_4 + \alpha_1\alpha_3 - 1)$ represent the only two relevant design parameters. The solutions $\cos \theta_{1,2}$ of (28) satisfy the quadratic equation

$$(29) \quad \chi_4 \cos^2 \theta - 2\Gamma_4 \cos \theta + (2\Gamma_4 - \chi_4 + 4) = 0.$$

For the special case of a homogeneous design ($\alpha_1 = \alpha_2 = \alpha_3 = \alpha_4 = 1$) we have that $\chi_4 = 16$ and $\Gamma_4 = 4$. Substituting these values into the quadratic equation (29), we find that the corresponding base angles $0 < \theta_1, \theta_2 < \pi$ relate to the golden ratio $w^2 - w - 1 = 0$, where $w = 2\cos(\theta) = z + \frac{1}{z} = \frac{1 \pm \sqrt{5}}{2}$. This further implies that $\theta_1 = \frac{\pi}{5}$ and $\theta_2 = \frac{3\pi}{5}$, which matches the regular distribution patterns for the optimal angles discussed in subsection 4.4. Although a five-layer design has four impedance ratios, (28) suggests that there are only two relevant design parameters. Generally, an m -layered design with $(m - 1)$ impedance ratios is expected to have $\lfloor \frac{m}{2} \rfloor$ distinct base angles and the same number of relevant design parameters. Notice the similar form of (26)–(28), (27)–(29), $|A_2|$ with $|A_3|$, and $|A_4|$ with $|A_5|$ in (45).

In summary, this approach provides the framework on how to recover necessary conditions for the base angle(s) and design parameter(s) for any given design, by displaying at the same time relations among the base angles themselves. However, applying this approach for a large number m of layers poses a computational challenge. Furthermore, a general pattern for the m -layer case is not easily recognized as it previously was in Approach 1, when D_m was described in (24).

4. Optimization results. Previously in (14)–(15) we described a finite trigonometric series representation for the stress in an elastic strip of m layers subjected to the Heaviside step in stress loading p at time $t = 0$ on one end and held fixed on the other end. We also discussed necessary conditions that the base angles and suitable design parameters must satisfy for a given m -layered design. Here we study optimal designs which provide the smallest stress amplitude throughout the strip for all time. These designs, besides the necessary conditions, will require additional conditions for the base angles and suitable design parameters to satisfy. In this section, we derive optimality conditions mainly for designs with a low number of layers. We know from (14) that

$$s_i(n) = s_i(n, p, \vec{\eta}_m)$$

for $i = 1, 2, \dots, m$, where $\vec{\eta}_m = (\alpha_1, \alpha_2, \dots, \alpha_{m-1})$. As a result, we formulate our optimal design problem as

$$(30) \quad \inf_{\vec{\eta}_m} \sup_{1 \leq n < +\infty} [p, s_1(n, p, \vec{\eta}_m), s_2(n, p, \vec{\eta}_m), \dots, s_m(n, p, \vec{\eta}_m)].$$

Considering the fact that one end of the strip is subjected to the loading p and that the homogeneous design ($\alpha_1 = \alpha_2 = \dots = \alpha_{m-1} = 1$) reaches the stress amplitude

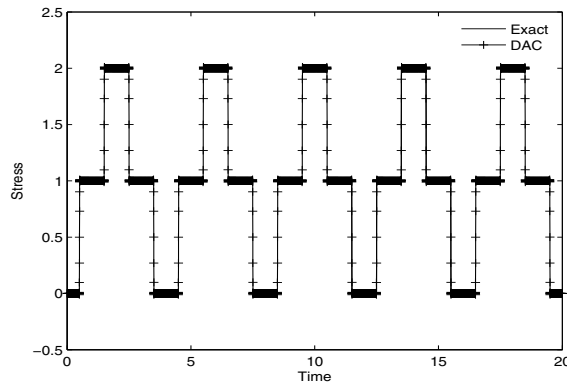


FIG. 2. Stress time history at the middle of a homogeneous elastic strip, with a stress amplitude of double the loading $p = 1$.

of $2p$ (see Figure 2), the following trivial upper and lower bounds can be obtained by inspection:

$$(31) \quad p \leq \inf_{\vec{\eta}_m} \sup_{1 \leq n < +\infty} [p, s_1(n, p, \vec{\eta}_m), s_2(n, p, \vec{\eta}_m), \dots, s_m(n, p, \vec{\eta}_m)] \leq 2p.$$

The time domain solutions shown in Figure 2 are found by numerical inversion of the Laplace transform using the Dubner–Abate–Crump (DAC) algorithm described by [10]. The effects of Gibbs’ phenomena are mitigated using the so-called Lanczos σ -factors with 512 terms and a tolerance equal to 10^{-3} ; see [17].

Furthermore, based on the value of the upper bound given in (31), the designs with $\chi_{m-1} = (1 + \alpha_1)(1 + \alpha_2) \cdots (1 + \alpha_{m-1}) < 2^{m-1}$ can never be optimal. This is due to the fact that the first transmitted stress wave (see (15)), after going through $m - 1$ layer interfaces and reflecting at the fixed boundary, reaches the value of $s_m(1) = s_m(n = 1, \vec{\eta}_m, p) = \frac{2^m}{\chi_{m-1}} p$, which is greater than $2p$ for $\chi_{m-1} < 2^{m-1}$. From this observation, our optimization problem (30) for the m -layer case equivalently reduces to

$$(32) \quad \inf_{\vec{\eta}_m, \chi_{m-1} \geq 2^{m-1}} \sup_{1 \leq n < +\infty} [p, s_1(n, p, \vec{\eta}_m), s_2(n, p, \vec{\eta}_m), \dots, s_m(n, p, \vec{\eta}_m)].$$

The first optimization results for this problem were obtained by [34] for the two-layer case with $m = 2$, where the class of optimal designs was identified. In the next subsections we will revisit these results using the stress representation (14)–(15) and discover similar optimality conditions for the media with low number of layers.

4.1. The two-layer case: Periodic optimal solutions. Based on the results of [34] for the two-layer case, the optimal designs are characterized by a stress amplitude of $2p$ and optimal values of the base angle $\theta_{1,opt}$ given by

$$(33) \quad \boxed{\theta_{1,opt} = \frac{\pi}{j}, \quad j = 2, 3, 4, \dots}$$

Substituting into (17), the corresponding optimal design parameter is

$$(34) \quad \boxed{\chi_{1,opt} = \frac{2}{1 - \cos(\theta_{1,opt})} = \frac{2}{1 - \cos \frac{\pi}{j}}, \quad j = 2, 3, 4, \dots}$$

TABLE 4.1

Numerical values of the optimal base angle and design parameter for the two-layer case.

j	2	3	4	5	6	7	8	9
$\theta_{1,opt}$	$\pi/2$	$\pi/3$	$\pi/4$	$\pi/5$	$\pi/6$	$\pi/7$	$\pi/8$	$\pi/9$
$\chi_{1,opt}$ (from (34))	2	4	6.828	10.472	14.928	20.196	26.274	33.163

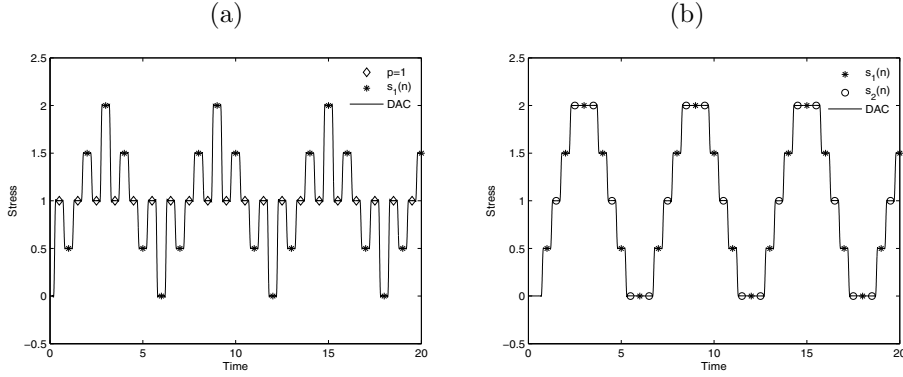


FIG. 3. Stress time history for a two-layered optimal design. Here the maximum stress amplitude is double the loading $p = 1$, while $j = 3$ and $\chi_{1,opt} = \frac{2}{(1-\cos(\frac{\pi}{j}))} = 4$ or $\alpha_{1,opt} = 3$. (a) Middle of the first layer located at $\xi = \tau/4$. (b) Middle of the second layer located at $\xi = 3\tau/4$.

where $\chi_{1,opt} = 1 + \alpha_{1,opt}$ and $\alpha_{1,opt}$ represents the impedance ratio of the optimal two-layered design. Notice that the class of optimal designs includes the homogeneous design obtained for $j = 2$, $\theta_{1,opt} = \pi/2$, and $\chi_{1,opt} = 2$. These optimality results are given in [34], and the first few values are displayed in Table 4.1. Based on the discussion in subsection 2.1, the values of the optimal base angle in (33) imply that the stress sequences $s_i(n)$, for a given $i = 1, 2$, are periodic functions with respect to $n \geq 0$. They share the same period $2j$ and circular frequency π/j , for $j = 2, 3, 4, \dots$. For example, when $j = 3$ the period is expected to be $2 \cdot 3 = 6$. Figures 3(a) and (b) confirm this expectation. The presence of only one base angle allows the stress sequences in (16) to be represented as a sinusoidal function of the form $\delta_i \sin(n\theta_1 + \phi_i) + \gamma_i$, $i = 1, 2$. Here ϕ_i represents the phase at $n = 0$, while δ_i , ϕ_i , and γ_i are constants, $i = 1, 2$. This explains the sinusoidal shape as well as the values for the period observed in the stress history graphs displayed in Figures 3(a)–(b) and in [34]. However, as shown by a counterexample in [34], not every design with periodic stress sequences is optimal.

4.2. The three-layer case: Periodic optimal solutions. Based on (18), the only design parameter that affects the stress values in the three-layer case is $\chi_2 = (1 + \alpha_1)(1 + \alpha_2)$. As a result in (32),

$$s_i(n) = s_i(n, p, \vec{\eta}_3) = s_i(n, p, \chi_2)$$

for $i = 1, 2, 3$ and $\vec{\eta}_3 = (\alpha_1, \alpha_2)$. Since the number of layers is odd ($m = 3$), the stress terms in (18) also involve $(-1)^n$ in addition to the linear combinations of sines and cosines; see (14)–(15). Knowing the stress terms, we find the optimality conditions for the three-layer case by using the same discrete optimization technique introduced by [34] for the two-layer case. Such optimality conditions imply optimal choices for the base angle θ_1 as well as design parameter χ_2 . Indeed, for a given $\chi_2 > 2^{3-1} = 4$

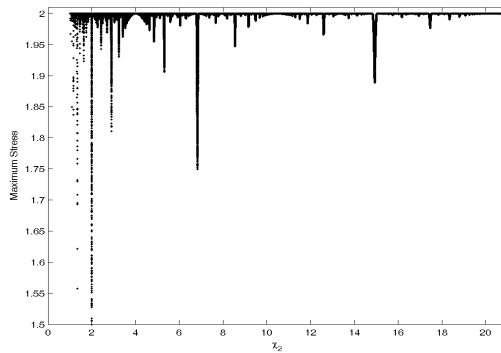


FIG. 4. Maximum value of the stress terms $s_1(n)$ for $0 \leq n \leq 300$ versus the design parameter $\chi_2 = (1 + \alpha_1)(1 + \alpha_2)$. The loading $p = 1$ while $0 < \alpha_1$ and $\alpha_2 < (\sqrt{21} - 1)$ are incremented by 0.005.

as stated in (32), one can derive analytically from the first equation of (18) that

$$(35) \quad 0 \leq s_1(n) = s_1(n, p, \chi_2) \leq 2p \quad \text{for all } n \geq 0.$$

This is illustrated in Figure 4. Similar to [34], from the second equation of (18) one can show that for any given three-layered design with $\chi_2 \geq 2^{m-1} = 2^{3-1} = 2^2$ there exists some value of n for which $s_2(n) = s_2(n, p, \chi_2) \geq 2p$. From there one can derive that the designs with $\max_{1 \leq n \leq \infty} s_2(n, p, \chi_2) = 2p$ satisfy $\sqrt{\chi_2 - 1} = \tan n\theta_1/2$ in addition to the necessary condition $\theta_1 = \arctan(\frac{2\sqrt{\chi_2-1}}{\chi_2-2})$ previously shown in subsection 2.2. This requires that $n\theta_1 = (2i + 1)\pi$ for all $i \geq 0$, which further implies that the designs with

$$(36) \quad \max_{0 \leq n < +\infty} s_2(n, p, \chi_2) = 2p$$

are characterized by the following parameters:

$$(37) \quad \theta_1 = \frac{\pi}{j}, \text{ or equivalently } \chi_2 = \frac{2}{1 - \cos(\theta_1)} = \frac{2}{1 - \cos(\frac{\pi}{j})}, \text{ for } j = 2, 3, 4, 5, \dots, \infty.$$

Figure 5(a) confirms these results, where the only three-layered designs that satisfy (36) have their values of χ_2 given by (37) for $j = 2, 3, \dots, 7$.

Finally, after a similar analysis of $s_3(n) = s_3(n, p, \chi_2)$ terms in the third equation of (18), due to the presence of $(-1)^n$ in their formulas, the sequence of optimal designs with the smallest stress amplitude of $2p$ remains to be the odd subsequence of (37). As illustrated in Figure 5(b), the only three-layered designs with

$$(38) \quad \max_{0 \leq n < +\infty} s_3(n, p, \chi_2) = 2p$$

have their values of χ_2 given by (37) for $j = 3, 5, 7$.

Putting together (35)–(38), for the three-layered elastic strip we identify the optimal base angles,

$$(39) \quad \boxed{\theta_{1,opt} = \frac{\pi}{j}, \quad j = 3, 5, 7, \dots,}$$

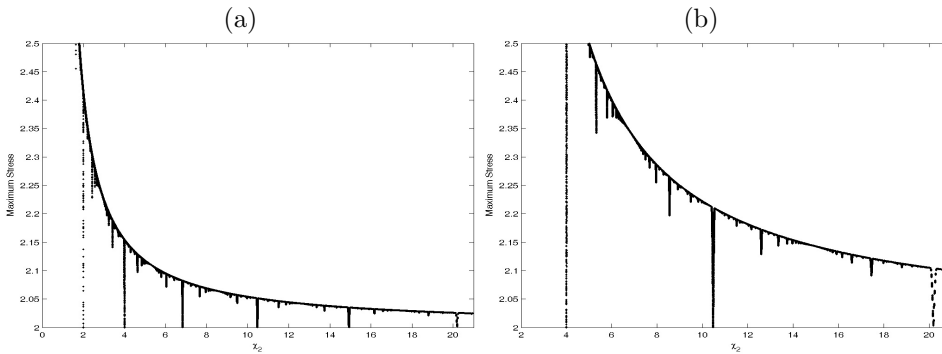


FIG. 5. Maximum value of the stress terms for $0 \leq n \leq 300$ versus the design parameter $\chi_2 = (1 + \alpha_1)(1 + \alpha_2)$. The loading $p = 1$ while $0 < \alpha_1$ and $\alpha_2 < (\sqrt{21} - 1)$ are incremented by 0.005. (a) The sequence $s_2(n)$. (b) The sequence $s_3(n)$.

and after substituting into (19), their corresponding optimal design parameters,

$$(40) \quad \chi_{2,opt} = \frac{2}{1 - \cos(\theta_{1,opt})} = \frac{2}{1 - \cos \frac{\pi}{j}}, \quad j = 3, 5, 7, \dots$$

These designs provide the smallest stress amplitude of $2p$ for the three-layered elastic strip and include the homogeneous design obtained for the first value of $j = 3$. As expected, $\chi_{2,opt} \geq 2^{m-1} = 2^{3-1} = 2^2 = \chi_{2,homog}$, where $\chi_{2,homog} = (1 + \alpha_1)(1 + \alpha_2) = (1 + 1)(1 + 1) = 2^2$ corresponds to the homogeneous design. Different designs with the same $\chi_{2,opt}$ share the same base angle. In other words, different layered designs can share the same set of optimal base angles. The first few numerical values of $\chi_{2,opt}$ are given in Table 4.2. Figures 5(a) and (b) have these values in common. It is important to notice that one can have infinitely many designs for the same value of χ_2 . Figure 6 displays curves obtained for the first few optimal values of χ_2 , representing optimal values for the pairs (α_1, α_2) . The first curve with $\chi_{2,opt} = 4$ includes the homogeneous design with $\alpha_1 = \alpha_2 = 1$. All the curves are symmetric with respect to the line $\alpha_2 = \alpha_1$; see subsection 5.1 for further discussion.

TABLE 4.2
Numerical values of the optimal base angle and design parameter for the three-layer case.

j	3	5	7	9
$\theta_{1,opt}$	$\pi/3$	$\pi/5$	$\pi/7$	$\pi/9$
$\chi_{2,opt}$ (from (40))	4	10.472	20.196	33.163

Based on the discussion in subsection 2.2, the values of the optimal base angle in (39) imply that the stress sequences $s_i(n)$, for a given $i = 1, 2, 3$, are periodic functions with respect to $n \geq 0$. Due to the fact that we have an odd number of layers ($m = 3$), the stress sequences share a common period which is an even integer $2j$. For example, when $j = 5$, the period is expected to be $2 \cdot 5 = 10$. Figures 7(a) and (b) confirm this expectation because they display ten terms of each stress sequence before the pattern repeats itself. One can also check by substituting into (18) that the stress sequences reach the maximum amplitude of $2p$ at half the period when $n\theta_{1,opt} = \pi$. As a result, the larger the odd values of j , the bigger the delay on the stress amplitude.

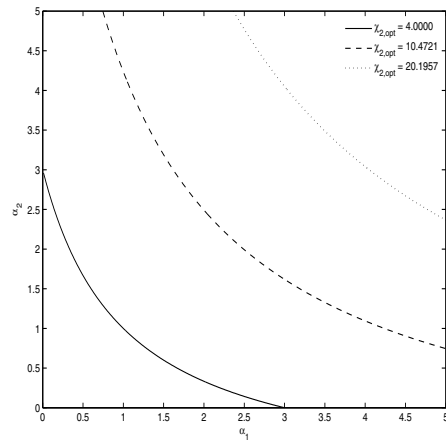


FIG. 6. Curves with equation $(1 + \alpha_1)(1 + \alpha_2) = \chi_{2,opt}$, generated for the first few values of $\chi_{2,opt}$ and representing optimal three-layered designs.

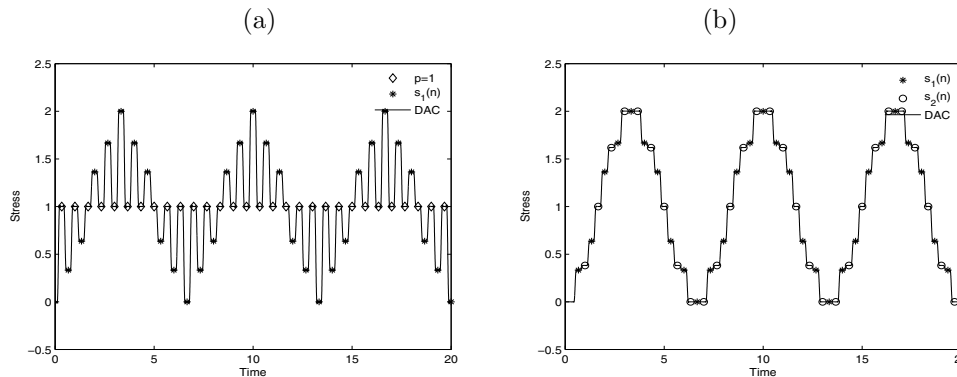


FIG. 7. Stress time history for the first two layers of a three-layered optimal design. Here the maximum stress amplitude is double the loading $p=1$, while $j = 5$, $\chi_{2,opt} = \frac{2}{(1-\cos(\frac{\pi}{j}))}$, and $\alpha_{1,opt} = 5$. (a) Middle of the first layer located at $\xi = \tau/6$. (b) Middle of the second layer located at $\xi = \tau/2$.

4.3. The four-layer case: Periodic solutions with amplitude $2p$. Heuristic optimization approach. For the case of four or more layers, the process of solving (5), which involves finding the coefficients in the trigonometric stress representation (14), becomes computationally challenging. Therefore, in the absence of the values of such coefficients, we will try to identify designs with the largest amplitude of $2p$ using the necessary conditions (26) derived from the z -space in section 3. However, we will no longer be able to rigorously prove as before that such designs are optimal.

We begin by using the necessary condition (26) for the base angles and suitable design parameters for the four-layer case. Our heuristic optimization approach in identifying designs with amplitude $2p$ is based on two facts:

1. The homogeneous design ($\alpha_1 = \alpha_2 = \alpha_3 = 1$) has a maximum amplitude of $2p$ and therefore is expected to be optimal just like in the two- and three-layer cases. This fact motivates us to substitute in (26.1) relation

$$\Gamma_3 = \alpha_1 \alpha_3 - 1 = 0,$$

which holds true for a homogeneous design and implies

the following (optimal) condition between the two base angles:

$$(41) \quad \boxed{\cos \theta_1 = -\cos \theta_2.}$$

Substituting back into the second equation of (26) gives

$$(42) \quad \chi_3 = \frac{2^2}{\sin^2 \theta_1} = \frac{2^3}{1 - \cos(2\theta_1)} = \frac{2^3}{1 - \cos(\tilde{\theta})},$$

where $0 < \tilde{\theta} = 2\theta_1 \leq \frac{\pi}{2}$ and $\chi_3 = (1 + \alpha_1)(1 + \alpha_2)(1 + \alpha_3)$.

2. *The two-layer case is a special case of the four-layer case with $\alpha_1 = \alpha_3 = 1$; therefore we can apply the optimality results for the two-layer case, given in (34), to the four-layer problem.* As a result, putting together (34) and (42) after substituting $\alpha_1 = \alpha_3 = 1$, we obtain

$$1 + \alpha_{2,opt} = \frac{2}{1 - \cos(2\theta_1)} = \frac{2}{1 - \cos(\frac{\pi}{j})}.$$

This suggests the following optimal values for the base angle θ_1 ,

$$(43) \quad \boxed{\theta_{1,opt} = \frac{\pi}{2j}, \quad \text{where } j = 2, 3, 4, \dots,}$$

and the following optimal design parameters,

$$(44) \quad \begin{cases} \chi_{3,opt} = \frac{2^3}{1 - \cos(\frac{\pi}{j})}, & j = 2, 3, 4, \dots, \\ \Gamma_{3,opt} = 0. \end{cases}$$

As before, $\chi_3 = (1 + \alpha_1)(1 + \alpha_2)(1 + \alpha_3)$, $\Gamma_3 = \alpha_1 \cdot \alpha_3 - 1$, and $\alpha_1, \alpha_2, \alpha_3 > 0$. The designs described in (44) are tested through numerical experiments which have confirmed the stress amplitude of $2p$. Such (optimal) designs have only one essential base angle given in (43), as the second base angle can be obtained from relation (41). Unlike the two- and three-layer cases, the conditions (44) are derived heuristically and do not necessarily describe the class of optimal designs. For the four-layer case, the first few optimal values of the design parameter $\chi_{3,opt}$ are displayed in Table 4.3. As expected from (34) and (44), and seen in Tables 4.1 and 4.3, the optimal values $\chi_{3,opt}$ for the four-layer case are $2^2 = 4$ times bigger than $\chi_{1,opt}$ for the two-layer case.

TABLE 4.3

Proposed numerical values of the optimal (essential) base angle and design parameter for the four-layer case.

j	2	3	4	5	6	7	8	9	10
$\theta_{1,opt}$	$\pi/4$	$\pi/6$	$\pi/8$	$\pi/10$	$\pi/12$	$\pi/14$	$\pi/16$	$\pi/18$	$\pi/20$
$\chi_{3,opt}$ from (44)	8	16	27.314	41.888	59.713	80.783	105.096	132.654	163.454

Similar to the three-layer case, based on (44), one can create many designs with amplitude $2p$ for the four-layer case. Once the value of α_1 is selected, a large enough optimal value of the design parameter $\chi_{3,opt}$ is selected from (44), so that the values of the remaining parameters, determined as $\alpha_3 = \frac{1}{\alpha_1}$ and $\alpha_2 = \frac{\chi_{3,opt}}{(1+\alpha_1)(1+\alpha_3)} - 1$, are

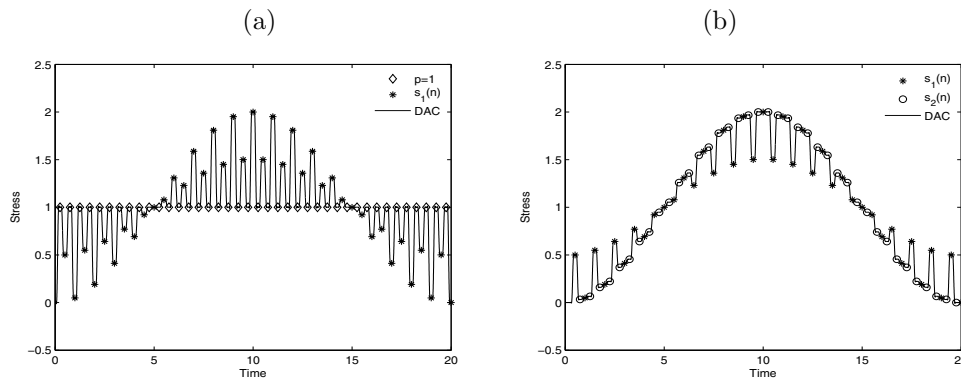


FIG. 8. Stress time history for the first two layers of a four-layered design with a maximum stress amplitude of double the loading $p = 1$. Here $j = 10$, $\chi_{3,opt} = \frac{2^3}{1 - \cos(\frac{\pi}{j})}$, $\alpha_1 = 3$, and $\alpha_3 = \frac{1}{\alpha_1} = \frac{1}{3}$. (a) Middle of the first layer located at $\xi = \tau/8$. (b) Middle of the second layer located at $\xi = 3\tau/8$.

reasonable and positive. For example, for $\alpha_1 = 3$, $j = 10$, and $\chi_{3,opt} = \frac{8}{1 - \cos(\frac{\pi}{j})} = \frac{8}{1 - \cos(\frac{\pi}{10})} \approx 163.454$, we can then make the appropriate material selection by choosing the impedance ratios $\alpha_3 = 1/\alpha_1 = 1/3$ and $\alpha_2 = \frac{\chi_{3,opt}}{(1+\alpha_1)(1+\alpha_3)} - 1 \approx 29.647$. The length of each layer is adjusted according to the material properties, in order to provide equal wave travel time. The stress history for this design is displayed in Figure 8. Notice the periodicity of the stress wave, while the stress amplitude never exceeds the value $2p$. Based on the discussion on periodic solutions in section 2, the values of the optimal base angle in (43) imply that the stress sequences $s_i(n)$, for a given $i = 1, 2, 3, 4$, are periodic functions with respect to $n \geq 0$. Given the fact that the essential base angle $\theta_{1,opt}$ is of the form $\pi/2j$, the common period for the stress sequences must be $4j$, while the circular frequency is the essential base angle $\pi/2j$. This agrees with the graphical output displayed in Figures 8(a) and (b). When $j = 10$ the period is expected to be $4 \cdot 10 = 40$; i.e., there are forty terms of each stress sequence before the pattern repeats itself. A delay benefit on the stress amplitude is also expected as the j index increases.

4.4. The multilayer case: Conjectures on periodic solutions with amplitude $2p$. As seen from (33), (39), and (43), the first optimal set of angles for the m -layer case is obtained when $j = m$ and $\theta_{1,opt} = \frac{\pi}{m}$, for $m = 2, 3, 4$. Notice the regular geometrical pattern of the optimal angle/root distribution on the unit circle displayed in Figure 9. Substituting into (45) the first set of optimal parameter values obtained for $j = m$ when $m = 2, 3, 4$ reduces it to $|A_m| = z^m + 1 = 0$, as expected. One can easily check that this class of optimal parameters with $\chi_{m-1,opt} = 2^{m-1}$ includes the homogeneous design obtained for $\alpha_1 = \alpha_2 = \dots = \alpha_{m-1} = 1$. We generalize the above observations with the following conjecture.

CONJECTURE 1. For the initial-boundary value problem discussed in this paper and a given integer $m \geq 1$, there are optimal m -layered designs, other than the homogeneous, for which $|A_m| = z^m + 1 = 0$ and $\chi_{m-1} = 2^{m-1}$. The roots of this equation are vertices of a regular m -gon, while the essential base angle/root is $\theta_1 = \pi/m$. The stress sequences $s_i(n)$, $i = 1, 2, \dots, m$, are expected to be periodic with respect to $n \geq 0$ and share the same (integer) period. The maximum amplitude of the stress sequences

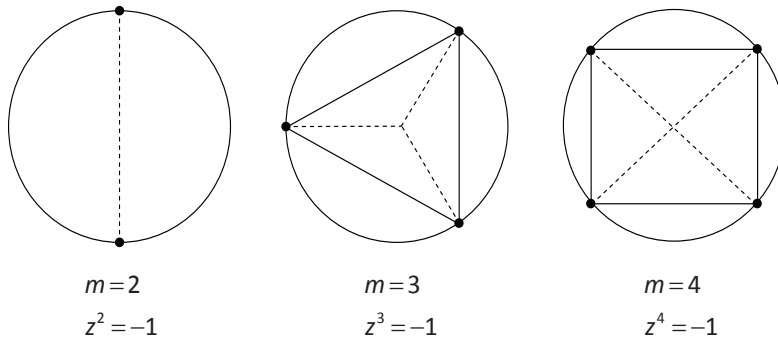


FIG. 9. Optimal angles derived from the roots of $z^m = -1$ for the m -layer case, $m = 2, 3, 4$.

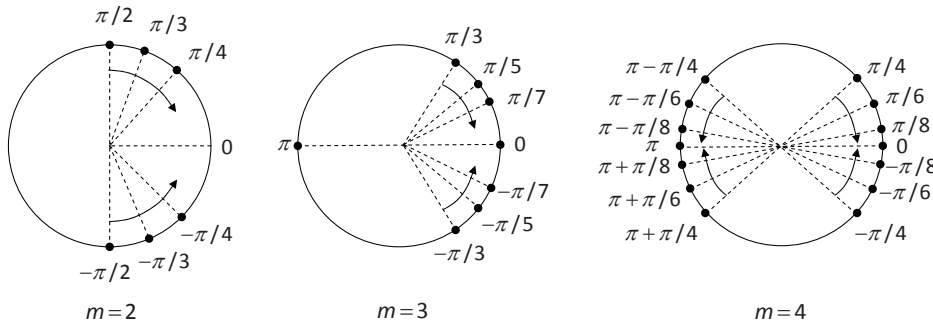


FIG. 10. Optimal angle distribution for the m -layer case, $m = 2, 3, 4$.

is expected to be double the loading p .

In Figure 10 we display the complete set of the optimal angles for the m -layer case obtained from (33), (39), and (43) when $j \geq m$ and $m = 2, 3, 4$. As we know, the four- and five-layer cases have two base angles.² Looking at the positioning and convergence tendency towards zero of these angles, we conjecture the following.

CONJECTURE 2. For the $m = 5$ layer case, the sets of angles $\{\pi, \pm\pi/(2j + 1), \pm(2j - 1)\pi/(2j + 1)\}$ for $j \geq 2$, combined with the necessary conditions (28) and other suitable base angle and design parameter relations, may generate (optimal) designs with maximum stress amplitude double the loading p . The stress sequences $s_i(n)$, $i = 1, 2, \dots, m$, are expected to be periodic with respect to $n \geq 0$ and share the same integer period, while $\chi_{m-1} \geq 2^{m-1}$.

As an application of Conjecture 2, we display in Figure 11 the stress history for a five-layered (optimal) design with maximum amplitude double the loading. The process of finding the numerical values of the (optimal) impedance ratios is described below. The design parameters χ_4 and Γ_4 are defined in terms of the impedance ratios as $\chi_4 = (1 + \alpha_1)(1 + \alpha_2)(1 + \alpha_3)(1 + \alpha_4)$ and $\Gamma_4 = (\alpha_1\alpha_3\alpha_4 + \alpha_1\alpha_2\alpha_4 + \alpha_1\alpha_4 + \alpha_2\alpha_4 + \alpha_1\alpha_3 - 1)$. From the necessary conditions (28) we can also express the design parameters χ_4 and Γ_4 in terms of the base angles: $\chi_4 = \frac{4}{1 - \cos\theta_1 - \cos\theta_2 + \cos\theta_1 \cdot \cos\theta_2}$ and

²Relation (41) between the two optimal base angles for $m = 4$ illustrated in Figure 10 explains why heuristic condition $\Gamma_3 = \alpha_1\alpha_3 - 1 = 0$ in subsection 4.3 worked.

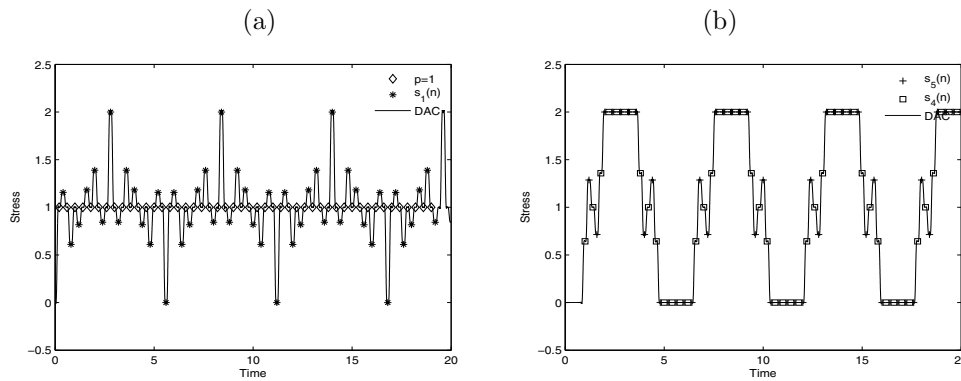


FIG. 11. Stress time history for the first and last layers of a five-layered design. Here the maximum stress amplitude is double the loading $p = 1$, while $j = 2$, $\theta_1 = \pi/(2j + 1) = \pi/7$, $\alpha_3 = 2$, $\alpha_4 = 1/\alpha_3 = 0.5$. (a) Middle of the first layer located at $\xi = \tau/10$. (b) Middle of the last layer located at $\xi = 9\tau/10$.

$\Gamma_4 = \frac{2(\cos\theta_1 + \cos\theta_2)}{1 - \cos\theta_1 - \cos\theta_2 + \cos\theta_1 \cdot \cos\theta_2}$. Substituting into the two different representations for χ_4 and Γ_4 the chosen values for $\alpha_3 = 2$ and $\alpha_4 = 1/\alpha_3 = 0.5$, and the assumed values for the base angles obtained for $j = 3$, $\theta_1 = \pi/(2j + 1) = \pi/7$ and $\theta_2 = (2j - 1)\pi/(2j + 1) = 5\pi/7$, we get a system of two equations and two unknowns α_1 and α_2 . As a result we recover the numerical values used for $\alpha_1 \approx 0.7291$ and $\alpha_2 \approx 2.1974$.

A general pattern of convergence of the base angles for the m -layered optimal designs with the smallest stress amplitude is yet to be found.

5. Applications of the optimality results. The properties of the materials used in this section are included in the appendix. Using the definition of the wave speed $c = \sqrt{E/\rho}$, the characteristic impedance ρc in each layer is calculated in terms of the material properties as $\sqrt{E\rho}$.

5.1. Multiple optimal material designs.

The two-layer case. According to (17), for a given value of the base angle θ_1 there is a unique corresponding value of $\chi_1 = 1 + \alpha_1$ and impedance ratio α_1 as a result. Furthermore, as shown in (33)–(34), optimal values of the base angle $\theta_{1,opt}$ generate optimal values for the design parameters $\chi_{1,opt}$ and $\alpha_{1,opt}$. When it comes to creating an optimal material design, this means that once one material is chosen for either layer, the properties of the material for the remaining layer are determined from the values of $\alpha_{1,opt}$. In other words, the optimal material selection has one degree of freedom. As for the length of each layer, it is adjusted according to the material properties in order to provide equal wave travel time: $\frac{L_1}{c_1} = \frac{L_2}{c_2}$ or $\frac{L_1}{L_2} = \sqrt{\frac{E_1}{\rho_1} \cdot \frac{\rho_2}{E_2}}$. Here L_i , c_i , E_i , and ρ_i , $i = 1, 2$, represent the length, wave speed, elastic modulus, and material density for the i th layer, respectively. For instance, if tungsten alloy is the material occupying the first layer, then the optimality condition $\chi_{1,opt} = \frac{2}{1 - \cos(\pi/4)} \approx 6.828$ or $\alpha_{1,opt} \approx 5.828$ is satisfied if the material in the second layer is lead. A different optimal value of $\chi_{1,opt} \approx 33.163$, or equivalently $\alpha_{1,opt} \approx 32.163$, is reached if the material in the second layer is copper alloy.

The three-layer case. Based on (19), for a given value of the base angle θ_1 , there is a unique corresponding value of $\chi_2 = (1 + \alpha_1)(1 + \alpha_2)$. Furthermore, as shown in

(39)–(40), optimal values of the base angle $\theta_{1,opt}$ generate optimal values for the design parameters $\chi_{2,opt}$. From (40), one can conclude that for a fixed value of α_1 there are infinitely many optimal designs. For a fixed value of $\chi_{2,opt}$ there are infinitely many optimal designs as well. The order of the impedance ratios does not matter; i.e., if $\alpha_1 = \alpha$ and $\alpha_2 = \beta$ represent an optimal design, $\alpha_1 = \beta$ and $\alpha_2 = \alpha$ represent an optimal design as well. The curves in Figure 6 confirm this expectation. Once the materials occupying the first two consecutive layers are selected, the value of α_1 is determined. The value of α_2 and the third material properties are then derived from the optimality conditions (40) for any value of $\chi_{2,opt}/(1 + \alpha_1) > 1$. Therefore when it comes to choosing optimal material design for the three-layer case, we have two degrees of freedom for material selection.

For instance, once we choose aluminum alloy and steel to occupy the first and second layer, respectively, the impedance ratio $\alpha_1 \approx .331$. Seeking values of $\chi_{2,opt}$ so that $\chi_{2,opt}/(1 + \alpha_1) > 1$, we choose $\chi_{2,opt} \approx 10.472$ and find the resulting impedance ratio $\alpha_2 = \frac{\chi_{2,opt}}{(1 + \alpha_1)} - 1 \approx 6.869$; see Table 4.2 and relation (40). From here we may choose various materials to occupy the third layer, one of them the glass fiber reinforced material. Theoretically, there are infinitely many optimal values with $\chi_{2,opt}/(1 + \alpha_1) > 1$ generated from (40) which provide even more (infinitely many) choices for the third material selection. Figure 6 illustrates the infinitely many choices for the optimal pairs (α_1, α_2) .

The four-layer case. In a similar fashion, based on (44) one can create multiple four-layer designs which are optimal. For instance, the homogeneous (optimal) design with $\alpha_1 = \alpha_2 = \alpha_3 = 1$ shares the same value of $\chi_{3,opt} = (1 + \alpha_1)(1 + \alpha_2)(1 + \alpha_3) = 2^3 = 8$ with the nonhomogeneous (optimal) design with $\alpha_1 = 2.5$, $\alpha_3 = 1/\alpha_1 = 0.4$, and $\alpha_2 = \frac{\chi_{3,opt}}{(1 + \alpha_1)(1 + \alpha_3)} - 1 \approx 0.633$. An optimal material selection for the four-layer case has two degrees of freedom.

Generally, it is important to mention that there is a potential gap between the theoretical predictions and what can be achieved practically. Some of the material properties required to create an optimal design might not correspond to an actual (elastic) material. Also, since the properties of the materials selected might have a slight deviation from the optimal values theoretically required, the designs created will be almost optimal.

5.2. Design improvement: Making a nonoptimal design optimal. One of the benefits of the optimality results for the layered strip is that they provide multiple options for optimal designs. This allows us to make an existing nonoptimal design optimal by adding or removing a (side) layer.

Reinterpreting the results discussed in the previous subsection, a nonoptimal two-layer strip can become optimal by adding a third layer with material properties determined by relations (40). Indeed, the aluminum-steel configuration for a two-layered design has an impedance ratio of $\alpha_1 \approx .331$, and therefore $\chi_1 = 1 + \alpha_1 \approx 1.331$. According to (34), this is a nonoptimal value for a two-layered Goupillaud-type strip. By adding a third layer of glass fiber reinforced material so that $\alpha_2 \approx 6.869$ and therefore $\chi_2 \approx 10.472$, according to (40), we obtain a nearly optimal configuration of three layers where $\chi_{2,opt} = \frac{2}{1 - \cos(\pi/5)} \approx 10.472$. The layer lengths are chosen so that they provide an equal wave travel time.

On the other hand, a three-layer design with tungsten-lead-aluminum configuration has impedance ratios $\alpha_1 \approx 5.828$, $\alpha_2 \approx 0.952$, and the nonoptimal design parameter $\chi_2 = (1 + \alpha_1)(1 + \alpha_2) \approx 13.33$; see Table 4.2 and (40). However, after we remove the aluminum alloy, the tungsten-lead combination with $\chi_1 = 1 + \alpha_1 = 6.828$

is an optimal design for the two-layer case.

Furthermore, an almost optimal four-layer configuration can be obtained by adding another layer as the first layer to the nonoptimal tungsten-lead-aluminum configuration with $\alpha_1 = 1/\alpha_3$, $\alpha_2 \approx 5.828$, and $\alpha_3 \approx 0.952$. The design parameter $\chi_3 = (1 + \alpha_1)(1 + \alpha_2)(1 + \alpha_3) \approx 27.32$ is close to the proposed (optimal) value of $\chi_{3,opt} = \frac{8}{1 - \cos(\pi/4)} \approx 27.314$; see (44) and Table 4.3.

Due to the round-off errors between the analytical predictions of the optimal design parameters and their calculated values, the material designs proposed here and created in practice are expected to be almost optimal. Our numerical experiments confirm stability in their behavior.

5.3. Optimization results for layered media with integer layer length ratios. The optimality results for Goupillaud-type layered media given in (40), (44) may be extended to non-Goupillaud-type layered media with integer layer length ratios. For instance, the optimality results in (40) for Goupillaud-type three-layered media can be extended to a non-Goupillaud-type two-layered media with 1:2 or 2:1 wave travel time ratios. The case with 1:2 ratio requires that $\alpha_2 = 1$ and $\alpha_{1,opt} = \frac{\cos \frac{\pi}{2j+1}}{1 - \cos \frac{\pi}{2j+1}}$, while the case with 2:1 ratio requires that $\alpha_1 = 1$ and $\alpha_{2,opt} = \frac{\cos \frac{\pi}{2j+1}}{1 - \cos \frac{\pi}{2j+1}}$ for $j \geq 1$.

Similarly, the proposed optimality conditions (44) for the Goupillaud-type four-layered media can be extended to three-layered media with wave travel time ratios 1:2:1 by choosing $\alpha_2 = 1$, $\alpha_3 = 1/\alpha_1$, and $(1 + \alpha_1)(1 + \alpha_3) = \frac{4}{1 - \cos(\pi/j)}$ for $j \geq 2$.

6. Summary and future work. A system of recursion relations that describe stress wave propagation in a multilayered Goupillaud-type elastic strip was derived. The system of equations was transformed using the z -transform method and written in a tridiagonal global matrix form. The determinant of the resulting global matrix was palindromic in nature. Under the assumption that the zeros of such a palindromic polynomial lie on the unit circle, we uniquely identified them by their angle measure. As a result, for an m -layered design there are m distinct angles: $\{\pm\theta_k\}_{k=1}^{\lfloor \frac{m}{2} \rfloor}$ when m is even and $\theta_0 = \pi$, $\{\pm\theta_k\}_{k=1}^{\lfloor \frac{m}{2} \rfloor}$ when m is odd. These correspond to their distinct complex conjugate roots on the unit circle. The angles $0 < \theta_k < \pi$ for $k = 1, \dots, \lfloor \frac{m}{2} \rfloor$ were known as the base angles. The stress wave propagation for the m -layered Goupillaud-type media was described in (14) by finite trigonometric series involving multiples of the base angles $\theta_1, \theta_2, \dots, \theta_{\lfloor \frac{m}{2} \rfloor}$. Formula (14) indicated that each stress term is a factor of the loading parameter p .

Necessary conditions for the base angles and design parameters for any given m -layered design were described. These conditions and the stress values found were affected only by $\lfloor \frac{m}{2} \rfloor$ base angles and the same number of suitable design parameters. The necessary conditions proved to be especially important for the designs of four or more layers for which we did not have the stress solutions. Substituting the optimal values of the base angles into the necessary conditions, combined with other suitable design parameter values, helped us identify sets of (optimal) designs with maximum stress amplitude of double the loading. The optimization results suggested regular distribution patterns of the optimal base angles. The stress sequences corresponding to optimal designs were periodic, shared the same period, and had nonnegative stress values for a positive/unit loading p . The applications of the optimality results discussed in section 5 were limited by the practical consideration of physically realizable values for the layer impedances. More work remains to be done in recovering optimal designs for the general case of m -layers.

Appendix.

A.1. Material properties. The elastic modulus E and density ρ of the materials used (see [1]) are as follows:

- Aluminum alloy: $E = 70$ GPa and $\rho = 2,500$ kg/m³,
- Copper alloy: $E = 10$ GPa and $\rho = 521.3$ kg/m³,
- Glass fiber reinforced material: $E = 30$ GPa and $\rho = 1,130$ kg/m³,
- Lead: $E = 14$ GPa and $\rho = 11,340$ kg/m³,
- Tungsten alloy: $E = 275$ GPa and $\rho = 19,610$ kg/m³,
- Steel: $E = 200$ GPa and $\rho = 8,000$ kg/m³.

A.2. The determinant of the tridiagonal matrix A_m . The determinant of the tridiagonal matrix A_m , given in (8), can be calculated using the formula $|A_m| = (z + 1)|A_{\{1, \dots, m-1\}}| - \eta_m \alpha_{m-1} \eta_{m-1} z |A_{\{1, \dots, m-2\}}|$. Here $|A_{\{1, \dots, l\}}|$ denotes the l th principal minor; that is, $A_{\{1, \dots, l\}}$ is the submatrix created by the first l rows and columns of A_m . The determinants $|A_m|$ for $1 \leq m \leq 5$, are given in (45):

$$\begin{aligned}
 |A_1| &= z + 1, \\
 |A_2| &= (z + 1)^2 - \eta_2 \eta_1 \alpha_1 z = z^2 - \frac{2(\chi_1 - 2)}{\chi_1} z + 1, \\
 |A_3| &= (z + 1)|A_{\{1,2\}}| - \eta_3 \alpha_2 \eta_2 z |A_{\{1\}}| = (z + 1) \cdot \left[z^2 - \frac{2(\chi_2 - 2)}{\chi_2} z + 1 \right], \\
 (45) \quad |A_4| &= (z + 1)|A_{\{1,2,3\}}| - \eta_4 \alpha_3 \eta_3 z |A_{\{1,2\}}| \\
 &= z^4 - \frac{4\Gamma_3}{\chi_3} z^3 + \frac{2(4\Gamma_3 - \chi_3 + 8)}{\chi_3} z^2 - \frac{4\Gamma_3}{\chi_3} z + 1, \\
 |A_5| &= (z + 1)|A_{\{1,2,3,4\}}| - \eta_5 \alpha_4 \eta_4 z |A_{\{1,2,3\}}| \\
 &= (z + 1) \cdot \left[z^4 - \frac{4\Gamma_4}{\chi_4} z^3 + \frac{2(4\Gamma_4 - \chi_4 + 8)}{\chi_4} z^2 - \frac{4\Gamma_4}{\chi_4} z + 1 \right].
 \end{aligned}$$

Here $\chi_3 = (1 + \alpha_1)(1 + \alpha_2)(1 + \alpha_3)$, $\Gamma_3 = (\alpha_1 \alpha_3 - 1)$, $\chi_4 = (1 + \alpha_1)(1 + \alpha_2)(1 + \alpha_3)(1 + \alpha_4)$, and $\Gamma_4 = (\alpha_1 \alpha_3 \alpha_4 + \alpha_1 \alpha_2 \alpha_4 + \alpha_1 \alpha_4 + \alpha_2 \alpha_4 + \alpha_1 \alpha_3 - 1)$.

Acknowledgments. The authors would like to acknowledge Thomas Debaecker, a former student from the École Spéciale Militaire de Saint-Cyr, France, and Thomas Davis, a former student of the University of San Diego, for their valuable assistance in obtaining initial results for the three-layer case.

REFERENCES

- [1] M. F. ASHBY, *Materials Selection in Mechanical Design*, 2nd ed., Butterworth-Heinemann, Oxford, UK, 2000.
- [2] J. BABOROWSKI, *Microfabrication of piezoelectric MEMS*, J. Electroceramics, 12 (2004), pp. 33–51.
- [3] P. BASSERAS, S. M. GRACEWSKI, G. W. WICKS, AND R. J. D. MILLER, *Optical generation of high-frequency acoustic waves in GaAs/Al xGa1-xAs periodic multilayer structures*, J. Appl. Phys., 75 (1994), pp. 2761–2768.
- [4] A. BEN-MENAHEM AND S. J. SINGH, *Seismic Waves and Sources*, Springer-Verlag, New York, 1981.
- [5] L. M. BREKHOVSKIKH, *Waves in Layered Media*, Academic Press, New York, 1960.
- [6] J. C. BRONSKI AND Z. RAPTI, *Modulational instability for nonlinear Schrodinger equations with a periodic potential*, Dyn. Partial Differ. Equ., 2 (2005), pp. 335–355.

- [7] C. CETINKAYA, A. F. VAKAKIS, AND M. EL-RAHEB, *Axisymmetric elastic waves in weakly coupled layered media of infinite radial extent*, J. Sound Vibration, 182 (1995), pp. 283–302.
- [8] Y. CHENG AND X. LIU, *Specific multi-scattering process in acoustic cloak with multilayered homogeneous isotropic materials*, J. Appl. Phys., 104 (2008), paper 104911.
- [9] J. F. CLAERBOUT, *Fundamentals of Geophysical Data Processing, With Applications to Petroleum Prospecting*, McGraw–Hill, New York, 1976.
- [10] K. CRUMP, *Numerical inversion of Laplace transforms using a Fourier series approximation*, J. ACM, 23 (1976), pp. 89–96.
- [11] D. S. DRUMHELLER, *Introduction to Wave Propagation in Nonlinear Fluids and Solids*, Cambridge University Press, Cambridge, UK, 1998.
- [12] P. GOUPILLAUD, *An approach to inverse filtering of near-surface layer effects from seismic records*, Geophys., 36 (1961), pp. 754–760.
- [13] N. A. HASKELL, *The dispersion of surface waves on multilayered media*, Bull. Seismol. Soc. Amer., 43 (1953), pp. 17–34.
- [14] S. A. JEWELL, E. HENDRY, T. H. ISAAC, AND J. R. SAMBLES, *Tuneable Fabry-Perot etalon for terahertz radiation*, New J. Phys., 10 (2008), paper 033012.
- [15] E. I. JURY, *Theory and Application of the z-Transform Method*, John Wiley & Sons, New York, 1964.
- [16] L. KNOPOFF, *A matrix method for elastic wave problems*, Bull. Seismol. Soc. Amer., 54 (1964), pp. 431–438.
- [17] R. LAVERTY AND G. GAZONAS, *An improvement to the Fourier series method for inversion of Laplace transforms applied to elastic and viscoelastic waves*, Int. J. Comput. Methods, 3 (2006), pp. 57–69.
- [18] L. LOSONCZI, *On reciprocal polynomials with zeros of modulus one*, Math. Inequal. Appl., 9 (2006), pp. 289–298.
- [19] M. J. S. LOWE, *Matrix techniques for modeling ultrasonic waves in multilayered media*, IEEE Trans. Ultrasonics, Ferroelectrics, and Frequency Control, 42 (1995), pp. 525–542.
- [20] D. L. MACFARLANE AND E. M. DOWLING, *Z-domain techniques in the analysis of Fabry-Perot etalons and multilayer structures*, J. Opt. Soc. Amer., 11 (1994), pp. 236–245.
- [21] L. N. MAKARAVA, M. M. NAZAROV, I. A. OZHEREDOV, A. P. SHKURINOV, A. G. SMIRNOV, AND S. V. ZHUKOVSKY, *Fibonacci-like photonic structure for femtosecond pulse compression*, Phys. Rev. E, 75 (2007), paper 036609.
- [22] B. S. MORDUKHOVICH AND J.-P. RAYMOND, *Neumann boundary control of hyperbolic equations with pointwise state constraints*, SIAM J. Control Optim., 43 (2005), pp. 1354–1372.
- [23] A. NOWAKOWSKI, *Sufficient optimality conditions for dirichlet boundary control of wave equations*, SIAM J. Control Optim., 47 (2008), pp. 92–110.
- [24] N. T. NGUYEN, *Adjoint optimization of one-dimensional hyperbolic equations with constrained periodic boundary conditions*, Comput. Methods Appl. Mech. Engrg., 197 (2008), pp. 4683–4691.
- [25] K. OGATA, *Discrete-Time Control System*, Prentice–Hall, Englewood Cliffs, NJ, 1987.
- [26] Y. PARK AND K. C. PARK, *High-fidelity modeling of MEMS resonators-Part I: Anchor loss mechanisms through substrate*, J. Microelectromechanical Systems, 13 (2004), pp. 238–247.
- [27] W. L. PILANT, *Elastic Waves in the Earth*, Elsevier Science, New York, 1979.
- [28] J. G. PROAKIS AND D. G. MANOLAKIS, *Introduction to Digital Signal Processing*, Macmillan, New York, 1988.
- [29] CH. SKOKOS, *On the stability of periodic orbits of high dimensional autonomous Hamiltonian systems*, Phys. D, 159 (2001), pp. 155–179.
- [30] P. STOICA AND A. NEHORAI, *The poles of symmetric linear prediction models lie on the unit circle*, IEEE Trans. Acoustics Speech Signal Process., 34 (1986), pp. 1344–1346.
- [31] W. T. THOMSON, *Transmission of elastic waves through a stratified solid medium*, J. Appl. Phys., 21 (1950), pp. 89–93.
- [32] S. TREITEL AND E. A. ROBINSON, *Seismic wave propagation in layered media in terms of communication theory*, Geophys., 31 (1966), pp. 17–32.
- [33] A. F. VAKAKIS AND C. CETINKAYA, *Dispersion of stress waves in one-dimensional semi-infinite, weakly coupled layered systems*, Int. J. Solids Structures, 33 (1996), pp. 4195–4213.
- [34] A. P. VELO AND G. A. GAZONAS, *Optimal design of a two-layered elastic strip subjected to transient loading*, Int. J. Solids Structures, 40 (2003), pp. 6417–6428.
- [35] J. WEI, M. XIAO, AND F. ZHANG, *Super-resolution with a nonlinear thin film: Beam reshaping via internal multi-interference*, Appl. Phys. Lett., 89 (2006), paper 223126.
- [36] A. R. WEILY, K. P. ESSELLE, B. C. SANDERS, AND T. S. BIRD, *High-gain 1D EBG resonator antenna*, Microwave Optical Technol. Lett., 47 (2005), pp. 107–114.

NO. OF
COPIES ORGANIZATION

1 DEFENSE TECHNICAL
(PDF INFORMATION CTR
only) DTIC OCA
8725 JOHN J KINGMAN RD
STE 0944
FORT BELVOIR VA 22060-6218

1 DIRECTOR
US ARMY RESEARCH LAB
IMNE ALC HRR
2800 POWDER MILL RD
ADELPHI MD 20783-1197

1 DIRECTOR
US ARMY RESEARCH LAB
RDRL CIM L
2800 POWDER MILL RD
ADELPHI MD 20783-1197

1 DIRECTOR
US ARMY RESEARCH LAB
RDRL CIM P
2800 POWDER MILL RD
ADELPHI MD 20783-1197

ABERDEEN PROVING GROUND

1 DIR USARL
RDRL CIM G (BLDG 4600)

<u>NO. OF COPIES</u>	<u>ORGANIZATION</u>
1 (CD only)	DPTY ASSIST SCT FOR R&T SARD TT ASA (ACT) J PARMENTOLA THE PENTAGON RM 3E479 WASHINGTON DC 20310-1714
1	PRIN DPTY FOR TCHNLGY HQ US ARMY MATCOM AMCDCGR R PRICE 9301 CHAPEK RD FT BELVOIR VA 22060-5527
3	AIR FORCE ARMAMENT LAB AFATL DLJW W COOK D BELK J FOSTER EGLIN AFB FL 32542
2	NSF S MCKNIGHT G PAULINO 4201 WILSON BLVD STE 545 ARLINGTON VA 22230-0002
1	DARPA W COBLENZ 3701 N FAIRFAX DR ARLINGTON VA 22203-1714
1	DIRECTOR US ARMY ARDEC AMSRD AAR AEE W E BAKER BLDG 3022 PICATINNY ARSENAL NJ 07806-5000
2	US ARMY TARDEC AMSTRA TR R MS 263 K BISHNOI D TEMPLETON MS 263 WARREN MI 48397-5000
1	COMMANDER US ARMY RSRCH OFC AMSRD ARL RO EN B LAMATTINA PO BOX 12211 RESEARCH TRIANGLE PARK NC 27709-2211

<u>NO. OF COPIES</u>	<u>ORGANIZATION</u>
1	COMMANDER US ARMY RSRCH OFC AMSRD ARL RO MM J LAVERY PO BOX 12211 RESEARCH TRIANGLE PARK NC 27709-2211
1	COMMANDER US ARMY RSRCH OFC AMSRD ARL RO EM D STEPP PO BOX 12211 RESEARCH TRIANGLE PARK NC 27709-2211
5	NAVAL RESEARCH LAB E R FRANCHI CODE 7100 M H ORR CODE 7120 J A BUCARO CODE 7130 J S PERKINS CODE 7140 S A CHIN BING CODE 7180 4555 OVERLOOK AVE SW WASHINGTON DC 20375
1	DTRA M GILTRUD 8725 JOHN J KINGMAN RD FORT BELVOIR VA 22060
1	ERDC US ARMY CORPS OF ENGINEERS USACEGSL P PAPADOS 7701 TELEGRAPH RD ALEXANDRIA VA 22315
1	AFOSR NL F FAHROO 875 N RANDOLPH ST STE 325 RM 3112 ARLINGTON VA 22203
1	CLEMSON UNIV DEPT MECH ENGR M GRUJICIC 241 ENGRG INNOVATION BLDG CLEMSON SC 29634-0921
1	UNIV OF CALIFORNIA CTR OF EXCELLENCE FOR ADV MATLS S NEMAT NASSER SAN DIEGO CA 92093-0416

<u>NO. OF COPIES</u>	<u>ORGANIZATION</u>	<u>NO. OF COPIES</u>	<u>ORGANIZATION</u>
5	DIRECTOR LANL P MAUDLIN R GRAY W R THISSELL A ZUREK F ADDESSIO PO BOX 1663 LOS ALAMOS NM 87545	2	SRI INTERNATIONAL D CURRAN D SHOCKEY 333 RAVENSWOOD AVE MENLO PARK CA 94025
7	DIRECTOR SANDIA NATL LABS J BISHOP MS 0346 E S HERTEL JR MS 0382 W REINHART MS 1181 T VOGLER MS 1181 L CHHABILDAS MS 1811 M FURNISH MS 1168 M KIPP MS 0378 PO BOX 5800 ALBUQUERQUE NM 87185-0307	1	VIRGINIA POLYTECHNIC INST COLLEGE OF ENGRG R BATRA BLACKSBURG VA 24061-0219
1	DIRECTOR LLNL M J MURPHY PO BOX 808 LIVERMORE CA 94550	8	UNIV OF NEBRASKA DEPT OF ENGRG MECH D ALLEN F BOBARU Y DZENIS G GOGOS M NEGAHBAN R FENG J TURNER Z ZHANG LINCOLN NE 68588
3	CALTECH M ORTIZ MS 105 50 G RAVICHANDRAN T J AHRENS MS 252 21 1201 E CALIFORNIA BLVD PASADENA CA 91125	1	JOHNS HOPKINS UNIV DEPT OF MECH ENGRG K T RAMESH LATROBE 122 BALTIMORE MD 21218
5	SOUTHWEST RSRCH INST C ANDERSON K DANNEMANN T HOLMQUIST G JOHNSON J WALKER PO DRAWER 28510 SAN ANTONIO TX 78284	4	UNIV OF UTAH DEPT OF MATH A CHERKAEV E CHERKAEV E S FOLIAS R BRANNON SALT LAKE CITY UT 84112
1	TEXAS A&M UNIV DEPT OF MATH J WALTON COLLEGE STATION TX 77843	1	PENN STATE UNIV DEPT OF ENGRG SCI & MECH F COSTANZO UNIVERSITY PARK PA 168023
1	WORCESTER POLYTECHNIC INST MATHEMATICAL SCI K LURIE WORCESTER MA 01609	3	UNIV OF DELAWARE DEPT OF MECH ENGRG T BUCHANAN T W CHOU M SANTARE 126 SPENCER LAB NEWARK DE 19716

<u>NO. OF COPIES</u>	<u>ORGANIZATION</u>	<u>NO. OF COPIES</u>	<u>ORGANIZATION</u>
1	UNIV OF DELAWARE CTR FOR COMPST MATRLS J GILLESPIE NEWARK DE 19716	2	WASHINGTON ST UNIV INST OF SHOCK PHYSICS Y M GUPTA J ASAY PULLMAN WA 99164-2814
1	COMPUTATIONAL MECH CONSULTANTS J A ZUKAS PO BOX 11314 BALTIMORE MD 21239-0314	1	NORTHWESTERN UNIV DEPT OF CIVIL & ENVIRON ENGRG Z BAZANT 2145 SHERIDAN RD A135 EVANSTON IL 60208-3109
1	LOUISIANA STATE UNIV R LIPTON 304 LOCKETT HALL BATON ROUGE LA 70803-4918	1	UNIV OF DAYTON RSRCH INST N S BRAR 300 COLLEGE PARK MS SPC 1911 DAYTON OH 45469
1	INST OF ADVANCED TECH UNIV OF TX AUSTIN S BLESS 3925 W BRAKER LN STE 400 AUSTIN TX 78759-5316	2	TEXAS A&M UNIV DEPT OF GEOPHYSICS MS 3115 F CHESTER T GANGI COLLEGE STATION TX 778431
1	APPLIED RSCH ASSOC D E GRADY 4300 SAN MATEO BLVD NE STE A220 ALBUQUERQUE NM 87110	1	UNIV OF SAN DIEGO DEPT OF MATH & CMPTR SCI A VELO 5998 ALCALA PARK SAN DIEGO CA 92110
1	INTERNATIONAL RSRCH ASSOC INC D L ORPHAL 4450 BLACK AVE PLEASANTON CA 94566	1	NATIONAL INST OF STANDARDS & TECHLGY BLDG & FIRE RSRCH LAB J MAIN 100 BUREAU DR MS 8611 GAITHERSBURG MD 20899-8611
3	ORNL ENVIRONMENTAL SCI DIV W DOLL T GAMEY L BEARD PO BOX 2008 OAK RIDGE TN 37831	1	MIT DEPT ARNTCS ASTRNTCS R RADOVITZKY 77 MASSACHUSETTS AVE CAMBRIDGE MA 02139
1	UNIV OF ILLINOIS DEPT OF MECHL SCI & ENGRG A F VAKAKIS 1206 W GREEN ST MC 244 URBANA CHAMPAIGN IL 61801	1	UNIV OF DELAWARE DEPT ELECTRICAL & CMPTR ENGRG D WEILE NEWARK DE 19716
1	UNIV OF ILLINOIS ARSPC ENGRG J LAMBROS 104 S WRIGHT ST MC 236 URBANA CHAMPAIGN IL 61801	2	MATERIALS SCI CORP A CAIAZZO R LAVERTY 181 GIBRALTAR RD HORSHAM PA 19044

NO. OF
COPIES ORGANIZATION

3 DIR USARL
RDRL D
V WEISS
RDRL SE
J PELLEGRINO
RDRL SES P
A EDELSTEIN
2800 POWDER MILL RD
ADELPHI MD 20783-1197

1 UNIV OF MISSISSIPPI
DEPT OF MECH ENGRG
A M RAJENDRAN
201 B CARRIER HALL
UNIVERSITY MS 38677

ABERDEEN PROVING GROUND

67 DIR USARL
RDRL WM
B FORCH
S KARNA
J MCCAULEY
P PLOSTINS
J SMITH
RDRL WML
J NEWILL
M ZOLTOSKI
RDRL WML B
I BATYREV
B RICE
N WEINGARTEN
RDRL WML D
P CONROY
M NUSCA
RDRL WML G
M BERMAN
W DRYSDALE
J ANDZELM
A RAWLETT
RDRL WML H
D SCHEFFLER
S SCHRAML
B SCHUSTER
RDRL WMM
R DOWDING
J ZABINSKI
RDRL WMM A
M MAHER
J TZENG
E WETZEL
RDRL WMM B
T BOGETTI
B CHEESEMAN
C FOUNTZOULAS
D HOPKINS

NO. OF
COPIES ORGANIZATION

B POWERS
C RANDOW
M VANLANDINGHAM
R WILDMAN
C F YEN
RDRL WMM D
E CHIN
K CHO
R HOWELL
RDRL WMM E
M COLE
T JESSEN
J LASALVIA
J SANDS
RDRL WMM F
L KECSKES
S MATHAUDHU
RDRL WMP
P BAKER
S SCHOENFELD
RDRL WMP B
R BECKER
S BILYK
D CASEM
J CLAYTON
C HOPPEL
M GREENFIELD
R KRAFT
B LEAVY
B LOVE
M SCHEIDLER
T WEERASOORIYA
RDRL WMP C
T BJERKE
S SEGLETES
RDRL WMP D
R DONEY
J RUNYEON
B SCOTT
RDRL WMP E
M BURKINS
RDRL WMP F
M CHOWDHURY
A FRYDMAN
N GNIAZDOWSKI
R GUPTA
RDRL WMP G
D KOOKER
G R PEHRSON